Am J Cancer Res 2023;13(5):2135-2154
www.ajcr.us /ISSN:2156-6976/ajcr0148973

Original Article

CNIH4: a novel biomarker connected with poor prognosis and cell proliferation in patients with lower-grade glioma

Feng Xiao[1,2,3,4*], Gufeng Sun[1,2,3,4*], Hong Zhu[1,2,3,4], Yun Guo[1,2,3,4], Fan Xu[5], Guowen Hu[1], Kai Huang[1,2,3,4], Hua Guo[1,2,3,4]

[1]Department of Neurosurgery, The Second Affiliated Hospital of Nanchang University, Nanchang 330006, Jiangxi, China; [2]Jiangxi Key Laboratory of Neurological Tumors and Cerebrovascular Diseases, Nanchang 330006, Jiangxi, China; [3]Jiangxi Health Commission Key Laboratory of Neurological Medicine, Nanchang 330006, Jiangxi, China; [4]Institute of Neuroscience, Nanchang University, Nanchang 330006, Jiangxi, China; [5]Department of Neurosurgery, People's Hospital of Nanchang County, Nanchang 330200, Jiangxi, China. [*]Equal contributors.

Received January 5, 2023; Accepted May 4, 2023; Epub May 15, 2023; Published May 30, 2023

Abstract: Cornichon family AMPA receptor auxiliary protein 4 (CNIH4) functions as an oncogene in several types of tumor. Nevertheless, the potential function of CNIH4 in lower-grade glioma (LGG) remains unclear. Pan-cancer analysis was implemented to comprehensively explore CNIH4 expression patterns and prognostic value in multiple cancers. Further, a systematic investigation of correlations between CNIH4 expression and clinical features, prognosis, biological functions, immune properties, genomic mutations, and treatment response was conducted, based on LGG expression patterns. CNIH4 expression levels and specific roles in LGG were also evaluated using *in vitro* experiments. Aberrant CNIH4 overexpression was detected in various tumors, and higher CNIH4 expression was linked with inferior prognosis, including in patients with LGG. Univariate and multivariate Cox regression analysis indicated that CNIH4 expression was an independent prognostic biomarker in patients with LGG. Our data also revealed that CNIH4 expression was strongly related to immune-associated signatures, immune cell infiltration, immune checkpoint genes, copy number alteration burden, tumor mutation burden, and treatment response in patients with LGG. *In vitro* experiments confirmed that CNIH4 was unusually elevated and crucial for cell proliferation, migration, invasion and cell cycle regulation in LGG. Together, our data validate CNIH4 may be an independent prognostic biomarker that could serve as a novel therapeutic target for improvement of prognosis in patients with LGG.

Keywords: CNIH4, lower grade glioma, prognosis, immune cell infiltration, treatment response, cell proliferation

Introduction

Glioma is a common primary intracranial tumor originating from glial cells [1]. The World Health Organization (WHO) categorizes gliomas as grade I to IV, based on their respective criteria [2], among which, grade II and III gliomas are deemed lower-grade gliomas (LGGs) by The Cancer Genome Atlas (TCGA). Currently, the most common regimens employed for clinical treatment of LGG include surgery, chemotherapy, and radiotherapy; however, few anticancer drugs are used to treat patients with LGG in the clinic, and the prognosis of these patients remains unsatisfactory. Therefore, exploration of new and effective treatments for patients with LGG is urgently needed.

CNIH4 is a member of the cornichon family of TGFα exporters that contributes to G protein-coupled receptor (GPCR) trafficking from the endoplasmic reticulum to the cell surface, where it promotes GPCR exit via the early secretory pathway. CNIH4 is regulated by TMED9 activity [3] and several studies have illustrated that raised CNIH4 expression is closely connected with the malignant development of several cancers, including liver [4], and colorectal cancers [3]; however, the role of CNIH4 in patients with LGG remains underexplored.

Therefore, we conducted this research to investigate the specific function of, and molecular mechanism involving, CNIH4 in patients with LGG.

First, we ascertained the prognostic role of CNIH4 in LGG by bioinformatics analysis of independent datasets from TCGA and the Chinese Glioma Genome Atlas (CGGA). Patients with LGG were grouped into low- and high-CNIH4 expression subtypes based on the median CNIH4 expression value. Survival analysis demonstrated that patients in the high-CNIH4 subgroup had shorter survival times than those in the low-CNIH4 subgroup. Receiver operating characteristic (ROC) curves and area under the curve (AUC) values were exploited to confirm the value of CNIH4 expression for predicting the prognosis of patients with LGG. By analyzing clinicopathological data from patients with LGG, we assessed whether there were associations between CNIH4 expression and age, sex, WHO grade, isocitrate dehydrogenase (IDH) status, chromosome 1p/19q codeletion (codel) status, and O6-methylguanine-DNA methyltransferase (MGMT) status. Moreover, Cox regression analyses were applied to explore whether CNIH4 expression is an independent prognostic biomarker in LGG. The underlying biofunctions of CNIH4 in LGG were scrutinized by functional enrichment analysis. Additionally, the single-sample gene set enrichment analysis (ssGSEA) algorithm was executed to examine associations between CNIH4 expression and 29 immune-related signatures. Additionally, we inspected associations between CNIH4 expression and immune traits, including tumor-infiltrating immune cells (TIICs), immune checkpoint genes (ICPGs), and stromal and immune scores; genomic alterations; and treatment response. Importantly, we also conducted *in vitro* experiments to examine the aberrant expression and specific functions of CNIH4 in LGG. Overall, the results of our comprehensive analyses demonstrate that CNIH4 is an independent prognostic biomarker in patients with LGG and may represent a novel therapeutic target in this context.

Methods

Data collation and management

Survival, mRNA expression, clinicopathological, and tumor mutation burden (TMB) data acquired from public databases were used for pan-cancer analysis. CNIH4 expression data and relevant clinical information from 33 tumors were obtained from TCGA database and CNIH4 expression data in normal tissue was collected from Genotype-Tissue Expression (GTEx).

In addition, two independent LGG datasets from TCGA and CGGA (CGGA_325) were analyzed in this research. RNA-seq expression data from the two datasets in fragments per kilobase million format, was transformed into transcripts per kilobase million values, then $\log_2$ transformed to facilitate comparison. Data on genomic variations in LGG samples were acquired from TCGA database.

Inclusion criteria for LGG samples

The following inclusion criteria were selected: 1) patients with WHO grade II and III tumors, 2) patients with mRNA sequencing data, and 3) overall survival (OS) ≥ 30 days. Data from 477 and 170 patients with LGG were screened from TCGA (**Table 1**) and CGGA (**Table 2**) databases, respectively. To ensure the congruity of survival data, data from 33 patients with LGG tumors and OS < 30 days were included in the CNIH4 pan-cancer analysis.

Prognostic role and validation of CNIH4

LGG samples were separated into low- and high-CNIH4 subtypes, based on median CNIH4 expression values in the two independent datasets. The prognosis of patients with LGG in the two subgroups was scrutinized by Kaplan-Meier analysis, and the value of CNIH4 expression for predicting the prognosis of patients with LGG in the two cohorts was estimated using survival rate, ROC curves, and AUC values. Subsequently, Cox regression analyses of the two cohorts were conducted to ascertain whether CNIH4 expression was an independent prognostic biomarker in patients with LGG.

Functional annotation and gene set variation analysis (GSVA)

The R package, limma [5], was exploited to identify differentially expressed genes (DEGs) between the low- and high-CNIH4 subgroups, with threshold values of $|\log_2$ fold-change (FC)$|$ > 0.5 and false-discovery rate (FDR) < 0.05. The R package, clusterProfiler [6], was employed to conduct gene ontology biological pro-

Table 1. Clinical features of LGG patients from TCGA

Clinical features		Total (477)	%
Age	Age ≤ 45	287	60.17%
	Age > 45	190	39.83%
Gender	Female	216	45.28%
	Male	261	54.72%
Grade	WHO II	231	48.43%
	WHO III	246	51.57%
1p/19q	Non-codel	321	67.30%
	Codel	156	32.70%
IDH	Mutant	389	81.55%
	Wildtype	85	17.82%
	Unknow	3	0.63%
MGMT	Unmethylated	82	17.19%
	Methylated	395	82.81%

Table 2. Clinical features of LGG patients from CGGA

Clinical features		Total (170)	%
Age	Age ≤ 45	129	75.88%
	Age > 45	41	24.12%
Gender	Female	65	38.24%
	Male	105	61.76%
Grade	WHO II	97	57.06%
	WHO III	73	42.94%
1p/19q	Non-codel	113	66.47%
	Codel	55	32.35%
	Unknow	2	1.18%
IDH	Mutant	125	73.53%
	Wildtype	44	25.88%
	Unknow	1	0.59%
MGMT	Unmethylated	70	41.18%
	Methylated	84	49.41%
	Unknow	16	9.41%

cess (GO-BP) and Kyoto Encyclopedia of Genes and Genomes (KEGG) analysis of DEGs. GSVA was implemented in R to identify pathways that were markedly enriched in the two subtypes [7]. The most enriched molecular pathways from the two subgroups were screened using KEGG (c2.cp.kegg.v7.2.symbols) genesets (threshold values: $\log_2$ FC > 0.1, P < 0.05, and FDR < 0.05).

Immunological traits of LGG

Immune features, such as stromal and immune scores, level of TIIC infiltration, and ICPGs expression level, were evaluated. First, the ssGSEA algorithm was implemented to estimate the differential enrichment of 29 immune-related factors, which were obtained from previous research [8], in the low- and high-CNIH4 subtypes. Consistent with gene expression profiles of patients with LGG, the ESTIMATE algorithm was exploited to inspect tumor purity and stromal and immune cell abundance [9] and to generate four score categories, as follows: ESTIMATE score (reflecting nontumor composites), immune score (reflecting the abundance of immune cells), stromal score (reflecting the abundance of stromal cells), and tumor purity. Subsequently, TIIC infiltration level was quantified using the CIBERSORT algorithm [10]. Additionally, based on previous research [11, 12], 25 ICPGs with potential therapeutic value were adopted and their correlations with CNIH4 expression determined.

Genetic mutation analysis

Deletions and amplification across the whole genome were evaluated using the RCircos tool [13] and compared between the low- and high-CNIH4 subtypes. Maftools [14] and GenVisR [15] were implemented to determine and visualize the types and frequencies of gene mutations between the two subgroups. TMB, as a novel biomarker of immunotherapy response, represents the total number of non-synonymous mutations. Associations between CNIH4 expression and TMB levels were assessed in 33 tumors using the R package, fmsb. Then, the R package, ggplot2, was implemented to examine the connection between CNIH4 expression and TMB levels in an independent TCGA LGG cohort.

Ethical approval

The medical ethics committee of the Second Affiliated Hospital of Nanchang University approved this research. All patients with LGG signed informed consent.

Cell culture and transfection

The LGG cell lines, BT142, SW1783, and SW1088, were obtained from the American Type Culture Collection. Normal human astrocyte (NHA) cells were from the Culture Collection of the Chinese Academy of Sciences (Shanghai, China). SW-1088, and SW-1783 cell lines were

cultured in Leibovitz's L-15 medium and 10% fetal bovine serum (Gibco). NHA and BT142 cell lines were cultured in Dulbecco's modified Eagle's medium/F12 medium. All cells were incubated at 37°C and in 5% carbon dioxide. SW1088 cells were transfected with shRNA and negative control (NC) lentiviral vectors, according to the protocol at a multiplicity of infection of 10. Positive cells were selected using puromycin. The *CNIH4* target sequence of shRNA was 5'-GCTGAAGTCACACATGAAAGA-3'.

Western blot analysis and quantitative real-time PCR (qRT-PCR)

Para-carcinoma and LGG tissue samples (n = 6 each) were collected from the second affiliated Hospital of Nanchang University and preserved in liquid nitrogen. Radioimmunoprecipitation analysis buffer (Solarbio, China) mixed with protease inhibitors was used to extract proteins from brain tissues and cell lysates. Then, lysates were separated by 10% SDS-PAGE and transferred to PVDF membranes for incubation with primary antibodies, including CNIH4 (1:50, sc-81857, Santa Cruz Biotechnology, China) and beta tubulin (1:2000, 10068-1-AP, Proteintech, China), followed by relevant secondary antibodies. Finally, membranes were incubated with enhanced chemiluminescence substrate (Thermo, USA) and visualized using the GV6000M imaging system (GelView6000pro). Total RNA was extracted from cells using a Simply P Total RNA Extraction Kit (Bioflux, China). Then, HiScript III-RT SuperMix (Vazyme, China) was employed to reverse-transcribe total RNA into complementary DNA. FC values were determined using the $2^{-\Delta\Delta CT}$ method. Primers sequences were as follows: CNIH4 forward, 5'-TTGCTCAAAATTAAACAAGTGGGT-3'; CNIH4 reverse, 5'-TTCCAAGTGGCAACAGGTAAGT-3'; beta tubulin forward, 5'-ACGCGGTTCTGTCTATCCAC-3'; and beta tubulin reverse, 5'-GAGGTGGTTATGCCGCTCAT-3'.

CCK-8 assays

Transfected SW1088 cells were plated in 96-well plates at 2×10^3 per well and cultured for 5 days. Next, 10 μL of CCK-8 assay reagent (Glpbio, GK10001) was added into each well and plates incubated for another 2 h, followed by measurement of absorbance at 450 nm.

Colony formation assays

Transfected SW1088 cells were seeded in 6-well plates at 2×10^3 per well and incubated for 2 weeks. Then, cells were stained with 0.1% crystal violet solution and the number of colonies quantified using ImageJ.

EdU assays

SW1088 cells (2×10^4 per well) were plated in 24-well plates and incubated for 72 h. Then, EdU reagents added and cells incubated for 2 h. Cells were fixed using 4% paraformaldehyde in 0.5% Triton X-100. Cells were then stained using Hoechst staining, and the EdU incorporation rate quantified using ImageJ.

Cell cycle analysis

Transfected SW1088 cells were fixed with 70% ethanol and stored at 4°C. Next, SW1088 cells were stained with propidium iodide/RNase Staining Buffer (Suzhou, China), and the distribution of the cells assessed by flow cytometry.

Cell migration and invasion assays

Transwell chambers (Corning) were coated in 500 μg/ml Matrigel (Yeasen) at 37°C for 30 min. Subsequently, SW1088 cells were plated at 5×10^4 per well and cultured in 100 μl serum-free medium. Leibovitz's L-15 medium containing 10% fetal bovine serum (600 μl) was added to the lower chambers of the transwell plates. After 24 h of culture, non-invasive cells were removed from transwell chambers using cotton swabs. Then, cells in chambers were fixed with 4% paraformaldehyde and stained with 0.1% crystal violet for 30 min. Finally, cells were imaged using a Leica Microsystems D-35578 microscope. Migration assays were conducted using the same method used for invasion assays, except for the absence of Matrigel at the bottom of the transwell chambers.

Assessment of CNIH4 expression and treatment response

The R package, pRRophetic [16], was executed to assess predicted differences in sensitivity to chemotherapeutic drugs, including PI3K/AKT inhibitors (A-443654, CAL-101, AKT inhibitor VIII, and TGX-221), proteasome inhibitors

(MG-132 and bortezomib), proteasome activators (Bryostain-1), and MAPK inhibitors (TAK-175), between the high- and low-CNIH4 subtypes.

Drug sensitivity assays

Transfected SW1088 cells were seeded in 96-well plates at 5×10^3 per well and incubated with chemotherapeutic drugs at different concentrations (0, 2, 4, 6, 8 μM). After incubating for 48 h, 10 μL of CCK-8 assay reagent (Glpbio, GK10001) per well was added and cells incubated for a further 2 h before measurement of absorbance at 450 nm.

Statistical analysis

Comparisons of clinical prognosis between patients in the high- and low-CNIH4 subtype groups were assessed by Kaplan-Meier analysis. AUC values and ROC curves were generated to ascertain the value of CNIH4 expression for predicting patient prognosis. Cox regression analysis was implemented to evaluate the independent prognostic value of CNIH4. Differences in 29 immune-related signatures, 25 ICPGs, TIICs, TMB, and copy number alteration (CNA) burden between the two subgroups were determined by Student's t test. In addition, correlations between variables were inspected by Pearson's or Spearman's correlation test. The Wilcoxon symbol-rank test was exploited to inspect the differences in predicted sensitivity to anticancer drugs between the two subgroups. All statistical analyses were implemented in R (version 4.1.0), SPSS Statistics, and GraphPad Prism 8 (GraphPad Software, Inc.). $P < 0.05$ was considered significant. All *in vitro* experiments were repeated three times independently.

Result

Pan-cancer analysis of CNIH4

The research processes used for this study are summarized in **Figure 1**. By comparing and analyzing pan-cancer data obtained from TCGA and GTEx datasets, we found that CNIH4 expression levels were abnormally high in various types of cancer. The results indicated that CNIH4 expression levels were evidently elevated in multiple tumors, including BLCA, BRCA, CHOL, COAD, GBM, HNSC, KIRC, KIRP, LGG, LIHC, PAAD, STAD, TGCT, and UCEC; and mildly elevated in CESC, LUSC, and READ (**Figure 2A**).

To inspect the prognostic value of CNIH4 in 33 tumor types, we implemented univariate Cox regression analysis to evaluate the association between CNIH4 expression and OS. As shown by Forest plots, high CNIH4 expression was negatively associated with OS in patients with CESC, HNSC, KIRP, LGG, LIHC, and PAAD (**Figure 2B**). Further, the results of survival analysis also demonstrated that patients with LGG and higher CNIH4 expression had inferior prognosis (**Figure 2C**).

Subsequently, we evaluated the relationships between CNIH4 expression and levels of ICPGs in 33 tumor types. The results of co-expression analyses demonstrated that CNIH4 was closely associated with the majority of ICPGs in BLCA, BRCA, COAD, ESCA, GBM, HNSC, LGG, LIHC, LUAD, LUSC, PAAD, PRAD, SKCM, STAD, THCA, and UCEC (**Figure 2D**). In addition, we examined the associations between CNIH4 expression and TMB in 33 cancers. In ACC, BLCA, BRCA, HNSC, LGG, LUSC, PAAD, PRAD, SKCM, STAD, THCA, THYM, and UCEC, CNIH4 expression was positively associated with TMB level, while in COAD, levels of CNIH4 expression were inversely associated with those of TMB (**Figure 2E**).

Association between CNIH4 and clinical traits in patients with LGG

The relationships between CNIH4 expression and clinicopathological variables (including age, gender, WHO grade, IDH, 1p/19q codel, and MGMT status) were inspected in TCGA and CGGA cohorts. The results demonstrated that upregulation of CNIH4 expression was strongly associated with older age, IDH wildtype status, 1p/19q non-codel status, and MGMT non-methylation status in TCGA cohort (**Figure 3A**, **3B**). We also detected similar results in the CGGA dataset (Figure S1A, S1B). Hence, CNIH4 expression level is tightly associated with clinicopathological characteristics in patients with LGG.

Elevated CNIH4 mRNA expression is associated with poor prognosis of patients with LGG

Kaplan-Meier analysis was implemented to detect differences in OS prognosis between high- and low-CNIH4 subgroups of patients with

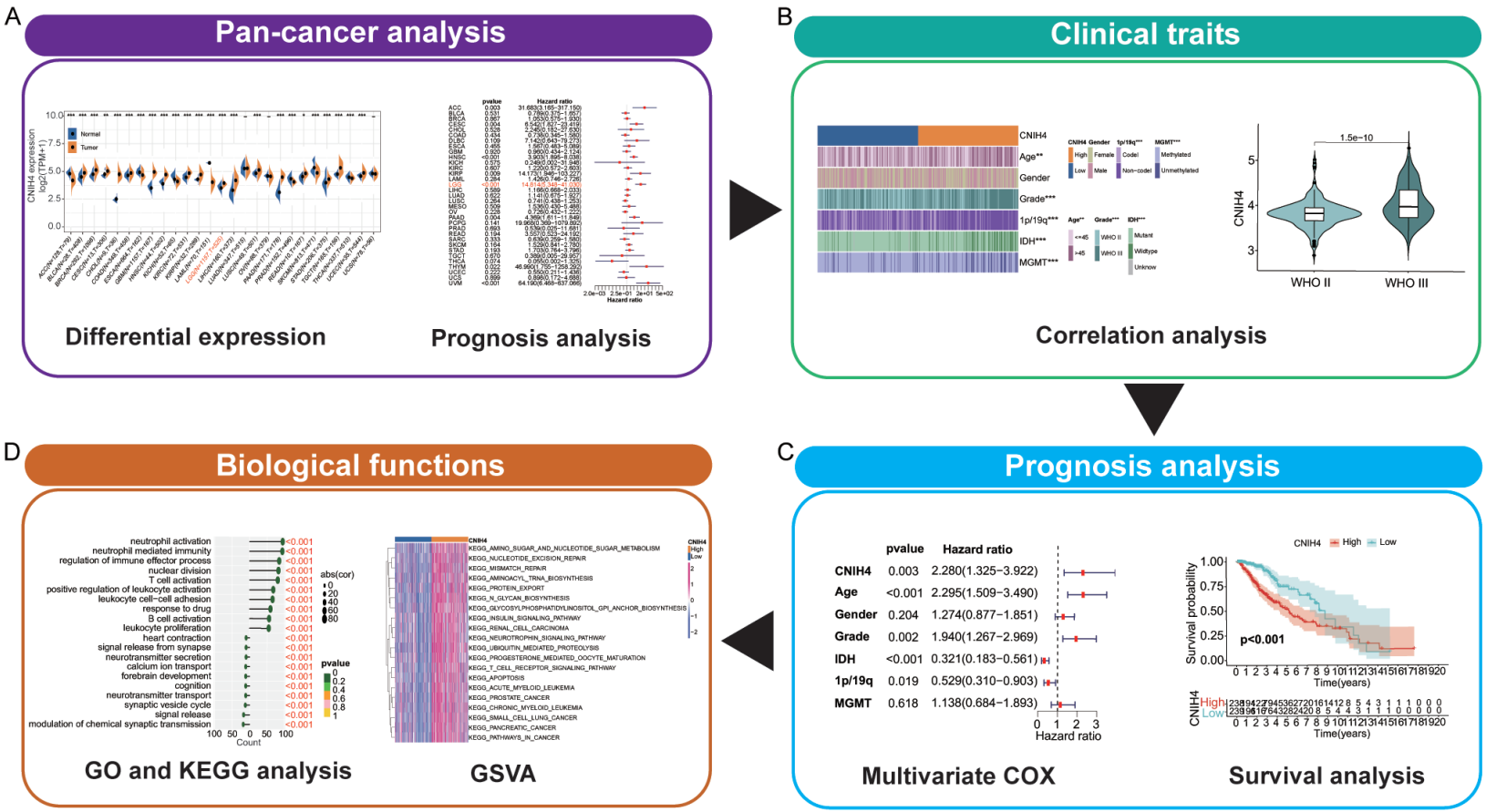
A
Pan-cancer analysis
Differential expression
Prognosis analysis
B
Clinical traits
Correlation analysis
C
Prognosis analysis
Multivariate COX
Survival analysis
D
Biological functions
GO and KEGG analysis
GSVA

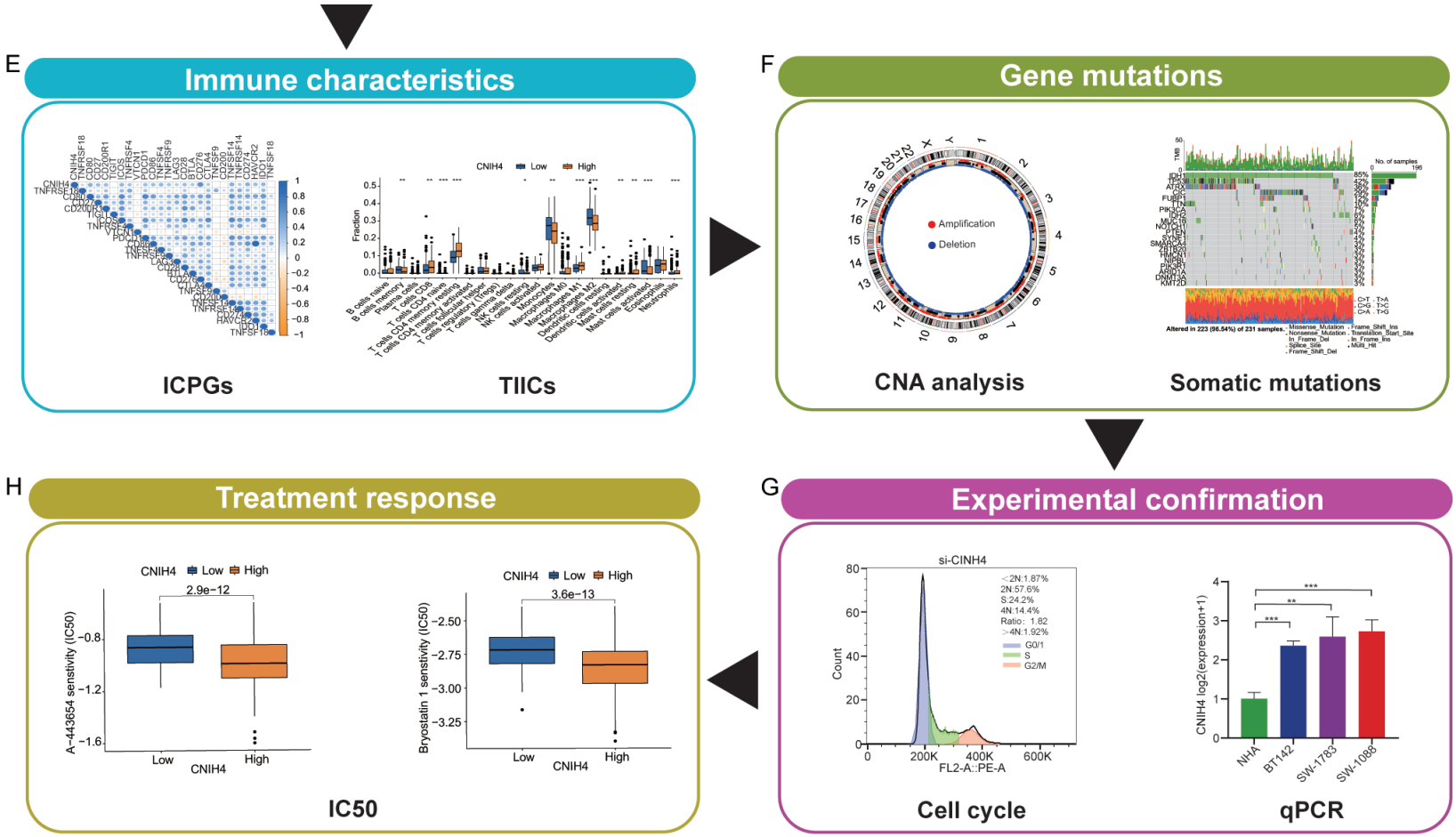

Figure 1. Overall study process for this research. A. Pan-cancer analysis. B. Clinical traits. C. Prognosis analysis. D. Biological functions. E. Immune characteristics. F. Gene mutations. G. Experimental confirmation. H. Treatment response of CNIH4 in LGG.

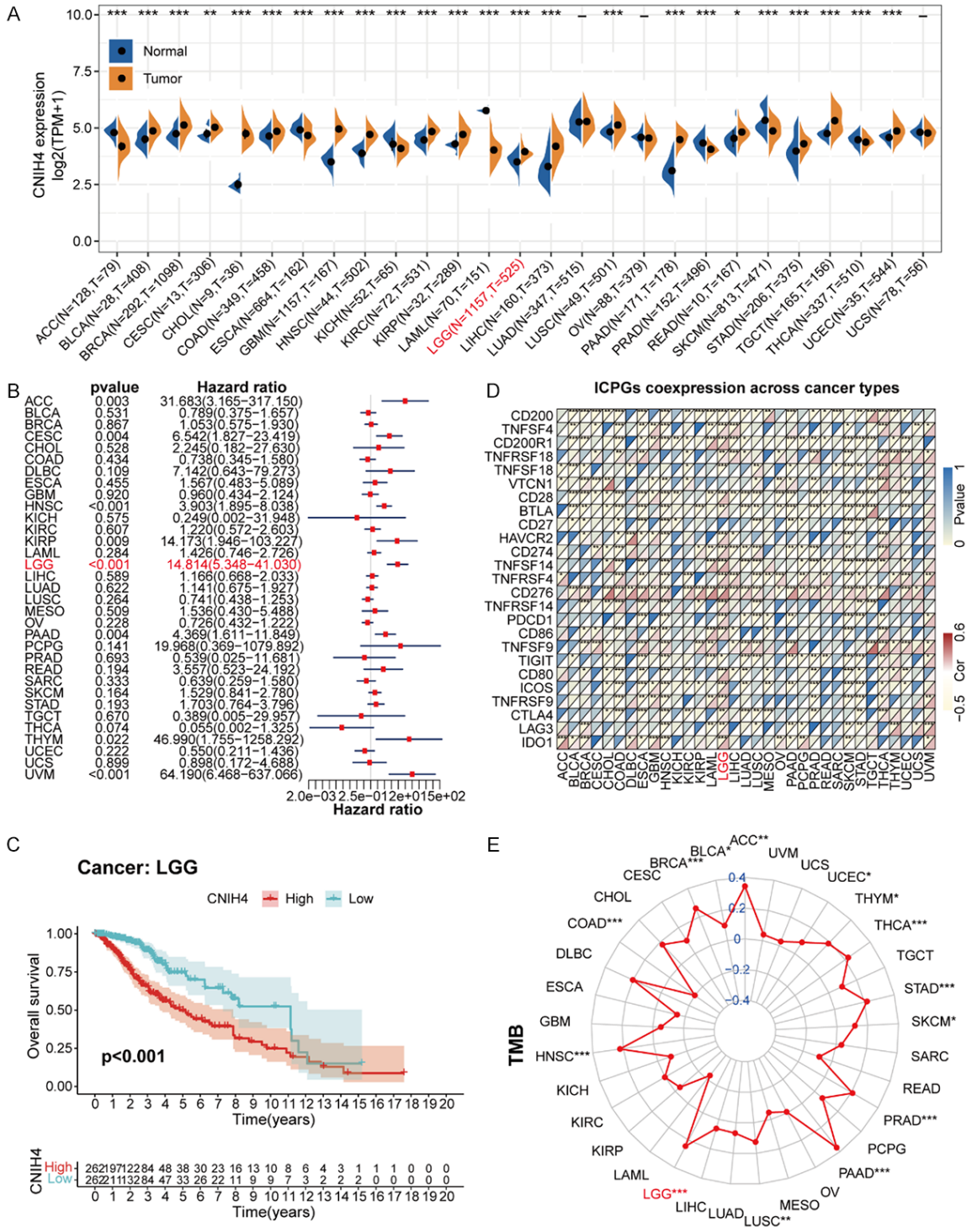

Figure 2. Pan-cancer analysis of CNIH4. A. Differential expression of CNIH4 in normal and cancer tissues. B. Univariate Cox regression analysis of CNIH4 expression in various tumors. C. Kaplan-Meier analysis of CNIH4 in pan-LGG. D. Co-expression of CNIH4 and ICPGs in different cancers. E. Differential TMB in diverse cancers. $^{*}P < 0.05$, $^{**}P < 0.01$, $^{***}P < 0.001$.

LGG. The results demonstrated that OS prognosis in the high-CNIH4 subgroup was notably worse than that in low-CNIH4 subtype in TCGA (**Figure 3C**) and CGGA (Figure S1C) data.

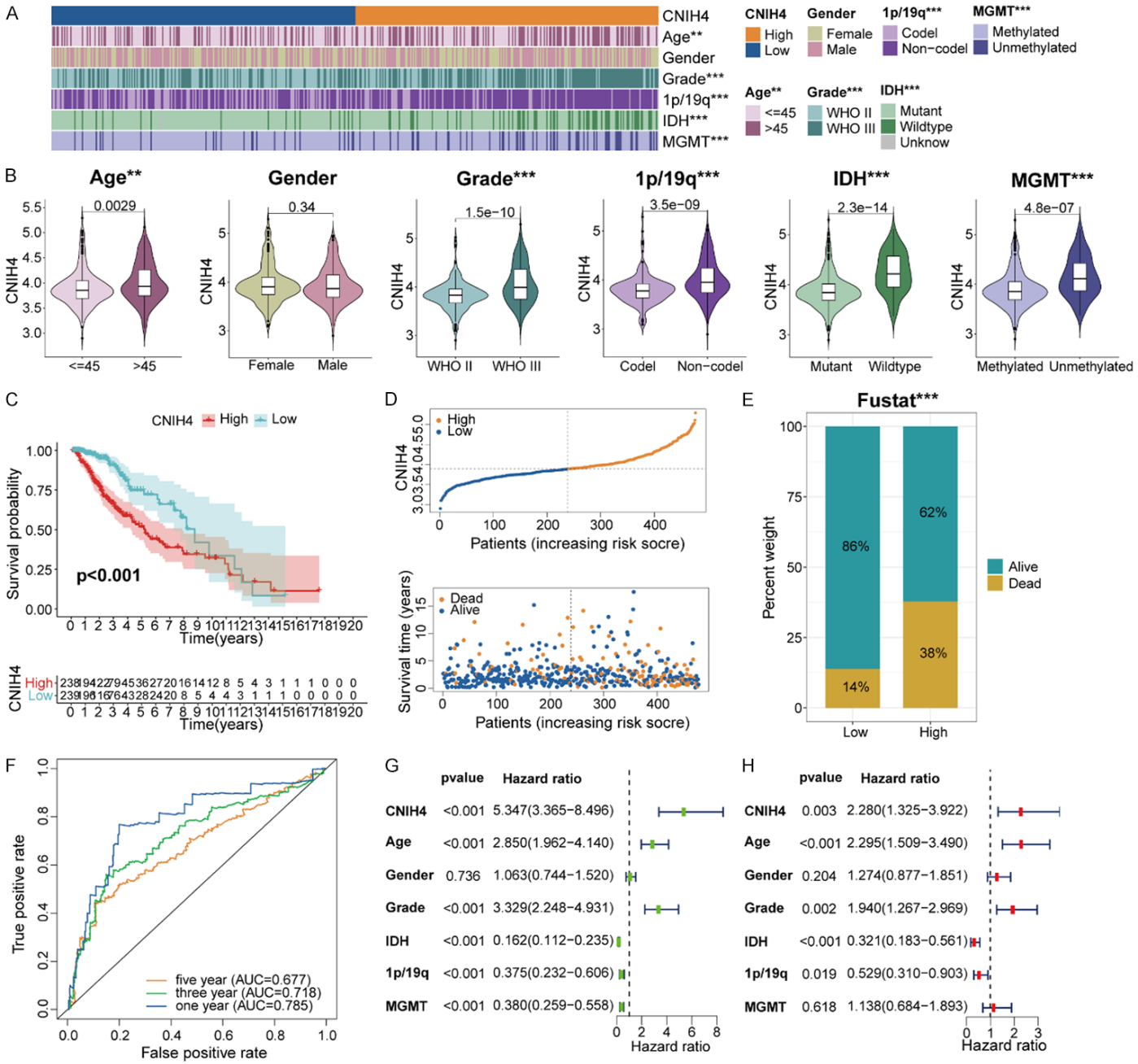
A
CNIH4
Age**
Gender
Grade***
1p/19q***
IDH***
MGMT***
CNIH4 High Low
Gender Female Male
1p/19q*** Codel Non-codel
MGMT*** Methylated Unmethylated
Age** <=45 >45
Grade*** WHO II WHO III
IDH*** Mutant Wildtype Unknow
B
Age** 0.0029 <=45 >45
Gender 0.34 Female Male
Grade*** 1.5e-10 WHO II WHO III
1p/19q*** 3.5e-09 Codel Non-codel
IDH*** 2.3e-14 Mutant Wildtype
MGMT*** 4.8e-07 Methylated Unmethylated
C
CNIH4 High Low
Survival probability
p<0.001
Time(years)
D
High Low
Patients (increasing risk socre)
Dead Alive
Survival time (years)
E
Fustat***
Percent weight
86% 14% 62% 38%
Alive Dead
Low High
F
True positive rate
False positive rate
five year (AUC=0.677)
three year (AUC=0.718)
one year (AUC=0.785)
G
pvalue Hazard ratio
CNIH4 <0.001 5.347(3.365-8.496)
Age <0.001 2.850(1.962-4.140)
Gender 0.736 1.063(0.744-1.520)
Grade <0.001 3.329(2.248-4.931)
IDH <0.001 0.162(0.112-0.235)
1p/19q <0.001 0.375(0.232-0.606)
MGMT <0.001 0.380(0.259-0.558)
Hazard ratio
H
pvalue Hazard ratio
CNIH4 0.003 2.280(1.325-3.922)
Age <0.001 2.295(1.509-3.490)
Gender 0.204 1.274(0.877-1.851)
Grade 0.002 1.940(1.267-2.969)
IDH <0.001 0.321(0.183-0.561)
1p/19q 0.019 0.529(0.310-0.903)
MGMT 0.618 1.138(0.684-1.893)
Hazard ratio

Figure 3. Clinical correlation analysis of CNIH4 in TCGA. A. Association between CNIH4 expression and clinical features of LGG in TCGA. B. Analysis of CNIH4 expression variation in patients with different clinical characteristics (including age, gender, tumor grade, and 1p/19q, *IDH*, and MGMT statuses) in TCGA dataset. C. Prognostic analysis of high- and low-CNIH4 subtypes in TCGA dataset. D. Distribution of risk score, OS, and OS status in high- and low-CNIH4 subtypes in TCGA dataset. E. Comparison of survival rates between the patients with LGG in the high- and low-CNIH4 subtypes. F. ROC curves illustrating the predictive value of risk score in TCGA data. G, H. Univariate and multivariate Cox analyses of CNIH4 expression and clinicopathological characteristics in TCGA. $^{*}P < 0.05$, $^{**}P < 0.01$, $^{***}P < 0.001$.

Therefore, we separately examined the connections between CNIH4 expression and risk score and OS status in patients with LGG and found that upregulation of CNIH4 expression was associated with higher risk score and poorer OS status in TCGA (**Figure 3D**) and CGGA (Figure S1D) cohorts. Detailed analysis of survival rates in patients with LGG demonstrated that those with high CNIH4 expression had inferior survival status in TCGA (**Figure 3E**) and CGGA (Figure S1E) cohorts. To validate the accuracy of CNIH4 level for predicting OS of patients with LGG in the two datasets, we conducted ROC curve analysis. AUC values for 1-, 3-, and 5-year OS were 0.785, 0.718, and 0.677 in TCGA dataset (**Figure 3F**), respectively; and 0.835, 0.877, and 0.833, respectively, in the CGGA dataset (Figure S1F). These results powerfully support the potential of CNIH4 as a valuable prognostic biomarker for patients with LGG.

Independent prognostic value of CNIH4

To examine whether CNIH4 was an independent prognostic biomarker in the two cohorts, we conducted univariate and multivariate Cox regression analyses. CNIH4 expression, WHO grade, and 1p/19q status were recognized as independent prognostic factors in both TCGA (**Figure 3G**, **3H**) and CGGA (Figure S1G, S1H) cohorts. Based on the results of univariate and multivariate Cox regression analysis of the two datasets, we infer that CNIH4 expression is an independent prognostic biomarker for predicting OS in patients with LGG.

Functional annotation of CNIH4

To scrutinize the potential role of CNIH4 in differential OS prognosis of patients with LGG, DEGs ($|\log_2 FC| > 0.5$ and $P < 0.05$) were identified between LGG with low- and high-CNIH4 expression, according to median expression value. A total of 263 down-regulated and 1481 up-regulated DEGs were detected in TCGA cohort, with 1593 down-regulated and 2462 up-regulated in the CGGA cohort. Heat maps were generated to visualize markedly DEGs in TCGA (**Figure 4A**) and CGGA (Figure S2A) cohort data.

Next, we conducted GO-BP and KEGG analyses of the up- and down-regulated DEGs. GO-BP results, based on analysis of up-regulated DEGs in TCGA cohort, demonstrated that those associated with up-regulated CNIH4 expression were chiefly enriched in neutrophil activation, regulation of immune response, T cell activation, B cell activation, and drug responses, among other processes. In addition, down-regulated CNIH4 expression was strongly connected with modulation of chemical synaptic transmission, signal release, synaptic vesicle cycle, neurotransmitter transport, and cognition (**Figure 4B**). Similar results were detected using the CGGA dataset (Figure S2B). KEGG analyses of TCGA (**Figure 4C**) and CGGA (Figure S2C) cohort data suggested that up-regulated DEGs were enriched in PI3K-Akt signaling, the cell cycle, MAPK signaling, TNF signaling, leukocyte transendothelial migration, NF-kappa B signaling, and B cell receptor signaling. Further, down-regulated DEGs were enriched in neuroactive ligand-receptor interaction, cAMP signaling, nicotine addiction, insulin secretion, glutamatergic synapse, and long-term potentiation.

To further evaluate the molecular pathways underlying the high- and low-CNIH4 LGG subtypes, we conducted GSVA of both TCGA and CGGA cohort data. The results suggested that the high-CNIH4 subtype was strongly interrelated with the T cell receptor signaling pathway and pathways in cancer in TCGA cohort (**Figure 4D**), with similar results in the CGGA cohort (Figure S2D). These results confirm that CNIH4 is closely associated with immune regulation in patients with LGG.

Associations between CNIH4 expression and immune characteristics

Our GO-BP and KEGG analyses of up-regulated DEGs suggested a strong association between CNIH4 levels and immune regulation in LGG.

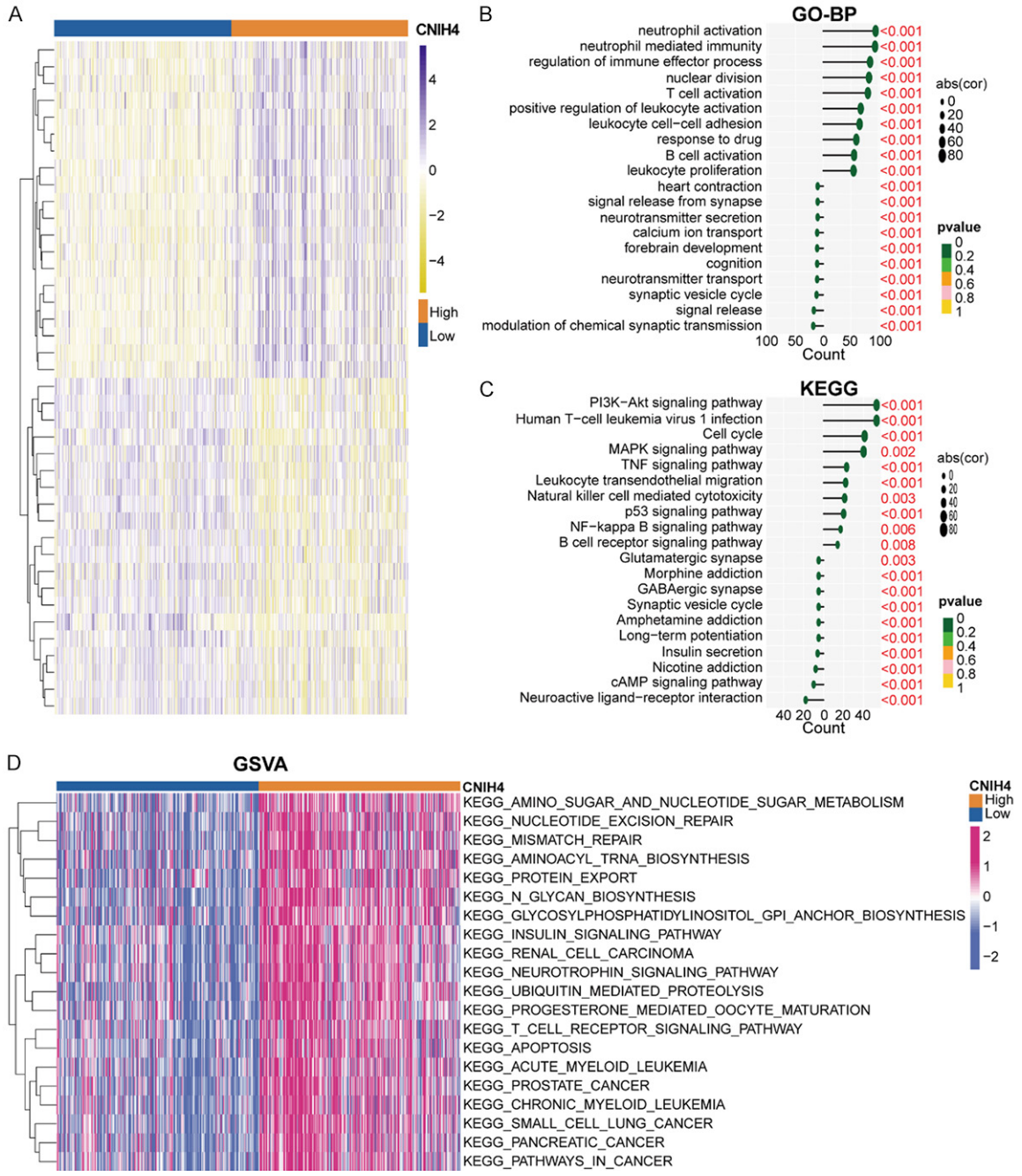

Figure 4. Biological functions of CNIH4 in LGG based on analysis of TCGA data. A. DEGs between the low- and high-CNIH4 expression LGG subgroups. B, C. GO-BP and KEGG analyses of CNIH4 expression-connected DEGs in patients with LGG in TCGA dataset. D. GSVA in TCGA dataset.

Therefore, we further evaluated the connection between CNIH4 and LGG immune traits using the ssGSEA algorithm, to assess enrichment for 29 immune-related signatures. In TCGA (**Figure 5A**) and CGGA (Figure S3A) cohort data, immune-related signatures were much more strongly enriched in the high-CNIH4 subtype than those in low-CNIH4 subtype. Additionally, CNIH4 expression was positively correlated with ESTIMATE, stromal, and immune scores, but inversely correlated with tumor purity in both TCGA (**Figure 5B**) and CGGA (Figure S3B) cohorts. Furthermore, we exploited the CIBERSORT algorithm to compare the abundance

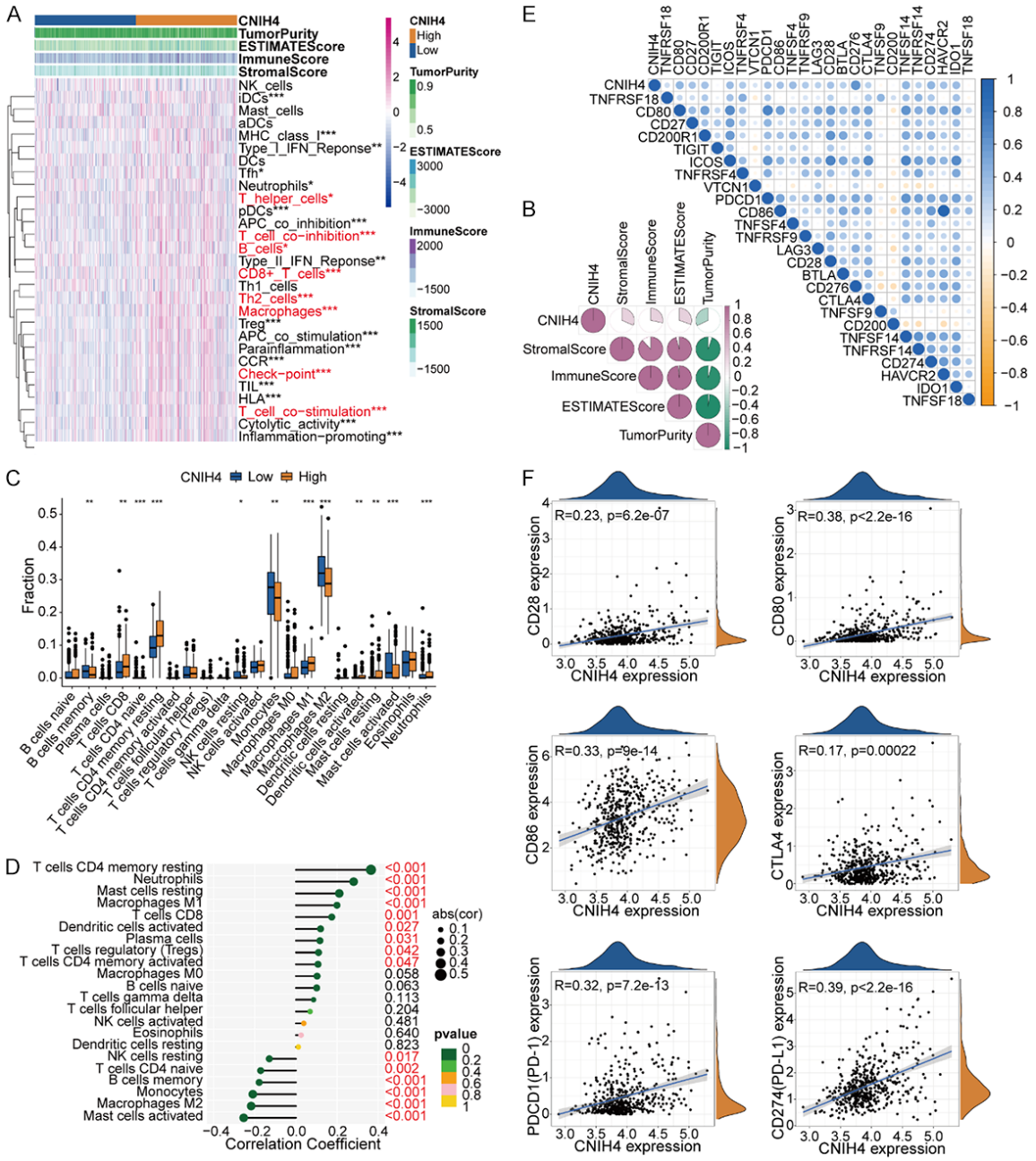

Figure 5. Different tumor microenvironment and immunological characteristics of the low- and high-CNIH4 subtypes in TCGA. A, B. Association between CNIH4 expression and 29 immune-associated signatures; ESTIMATE, immune, and stromal scores; and tumor purity. C. Comparisons of infiltration of 22 types of immune cells in the two subgroups. D. Lollipop plots showing the relationship between CNIH4 expression and TIICs. E, F. Co-expression analysis of CNIH4 and 25 ICPGs. $^{*}P < 0.05$, $^{**}P < 0.01$, $^{***}P < 0.001$.

of TIICs between the two subtypes. The abundances of infiltrating $CD8^{+}$ T, resting memory $CD4^{+}$ T, and M1 macrophage cells were positively correlated with CNIH4 expression in TCGA datasets. Meanwhile, memory B, naïve $CD4^{+}$ T, and macrophage M2 cell abundances were negatively correlated with CNIH4 expression (**Figure 5C**, **5D**). Similar results were obtained using CGGA cohort data (Figure S3C, S3D).

To further ascertain differences in expression of ICPGs and CNIH4 in patients with LGG, we

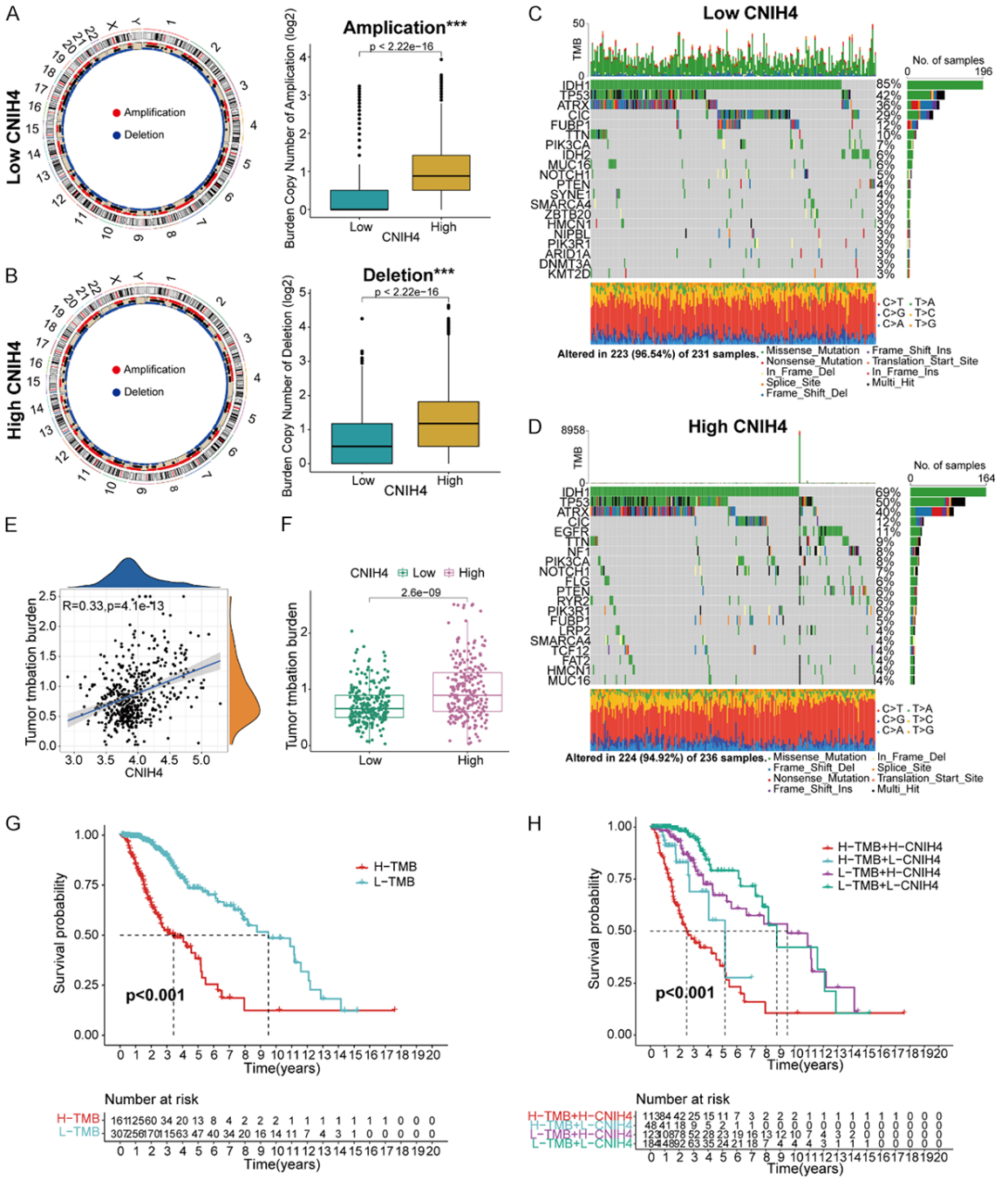

Figure 6. Comparison of genomic mutations in the two subgroups in TCGA dataset and *in vitro* experimental verification of disruption of CNIH4 expression in LGG. A, B. Circos plots of low-CNIH4 and high-CNIH4 subgroups illustrating chromosome amplifications and deletions, and boxplots showing a lower burden of copy number amplifications and deletions in the low-CNIH4 subgroup. C, D. Waterfall plots illustrating mutated genes in the low-CNIH4 and high-CNIH4 subgroups. E, F. Association between CNIH4 expression and TMB levels. G, H. Correlation between TMB level and the prognosis of patients with LGG and the differential prognostic value in the two subtypes with distinct TMB levels. $^{*}P < 0.05$, $^{**}P < 0.01$, $^{***}P < 0.001$.

conducted differential correlation analysis. In TCGA dataset, the results demonstrated that CNIH4 expression was positively correlated with that of the majority of ICPGs (**Figure 5E**). We also conducted correlation analysis of TCGA cohort data (**Figure 5F**) to analyze the detailed relationships between CNIH4 expression and levels of important ICPGs, including CD28, CD80, CD86, CTLA4, PD1, and PD-L1. Similar results were obtained using CGGA cohort data

(Figure S3E, S3F). These results provide strong evidence supporting a close association between CNIH4 expression level and the immune microenvironment.

CNIH4 expression is associated with CNIH4 genomic variations

There is considerable evidence that genomic mutations likely play critical roles in regulating tumor immunity [17-19]. To discern whether there were differences in genomic alterations between the low- and high-CNIH4 subtypes, we conducted CNA and somatic mutation analysis. The frequencies of amplification and deletion CNAs in the high-CNIH4 subgroup were clearly higher than those in the low-CNIH4 subtype (**Figure 6A**, **6B**). Further, somatic mutation analysis illustrated that the frequency of IDH1 and CIC mutations were higher in the low-CNIH4 subtype than in the high-CNIH4 subtype, while those of TP53 and ATRX were higher in the high-CNIH4 subgroup than in the low-CNIH4 subgroup (**Figure 6C**, **6D**). Moreover, we found that CNIH4 expression and TMB level were positively correlated (**Figure 6E**, **6F**). Analysis of variations in OS in patients with different CNIH4 expression in the low- and high-TMB subtypes demonstrated that higher CNIH4 expression and TMB levels were associated with inferior OS in patients with LGG (**Figure 6G**, **6H**). Therefore, CNIH4 expression may be closely correlated with genomic variation in patients with LGG.

Association between CNIH4 expression and treatment response

To assess the potential value of differences in CNIH4 expression in guiding chemotherapy for patients with LGG, we assessed the relationships between CNIH4 expression and response to chemotherapeutics, including A-443654, CAL-101, AKT inhibitor VIII, TGX-221, MG-132, bortezomib, Bryostain-1, and TAK-175, based on the results of functional annotation. Our findings indicated that high-CNIH4 expression was associated with lower half maximal inhibitory concentration values of these anticancer drugs (Figure S4), indicating that LGG with high CNIH4 expression is more sensitive to these anticancer drugs, which may, therefore, be useful chemotherapy agents in patients with LGG and high CNIH4 expression, with potential for future application.

In vitro analysis of CNIH4 levels in LGG

Levels of CNIH4 protein expression in LGG samples were notably higher than those in paracancerous samples, based on quantitative analysis using ImageJ software (**Figure 7A**). We also examined CNIH4 protein and mRNA expression in the LGG cell lines, BT142, SW1783, and SW1088, as well as in NHA cells, and found that CNIH4 levels were significantly higher in LGG than those in NHA cells (**Figure 7B**, **7C**).

Afterwards, we executed functional experiments to inspect the connection between CNIH4 expression and cell proliferation, migration, and invasion in LGG. CCK-8 assays illustrated that SW1088 cell viability in the si-CNIH4 group was clearly impaired relative to that in the si-NC group (**Figure 7D**). Colony formation assays suggested that CNIH4 downregulation evidently decreased cell colony formation relative to the si-NC group (**Figure 7E**, **7F**). EdU assays demonstrated that CNIH4 knockdown inhibited SW1088 cell proliferation (**Figure 7G**, **7H**). Further, cell cycle analysis suggested that CNIH4 downregulation induced cell cycle arrest (**Figure 7I**, **7J**). Transwell assays demonstrated that the migration and invasion capacities of the cells in the si-CNIH4 group were markedly diminished relative to those of the si-NC group (Figure S5A, S5B). These results illustrate that CNIH4 is vital for LGG cell proliferation, migration, and invasion. Additionally, drug sensitivity assays demonstrated that cells in the si-NC group were more sensitive to the chemotherapeutic drugs tested, including CAL-101 (Figure S5C), TGX-221 (Figure S5D), and TAK-175 (Figure S5E), than those in the si-CNIH4 group.

Discussion

Although considerable progress has been achieved through surgery, chemotherapy, and radiotherapy, the survival prognosis of patients with LGG remains wretched [20-23]. As the effect of conventional treatment on patients with LGG is limited, identification of novel therapeutic targets is necessary. CNIH4, a member of the cornichon family of TGFα exporters, is a key factor in regulation of cell proliferation. Numerous studies have demonstrated that raised CNIH4 expression can promote the malignant progression of several tumors; how-

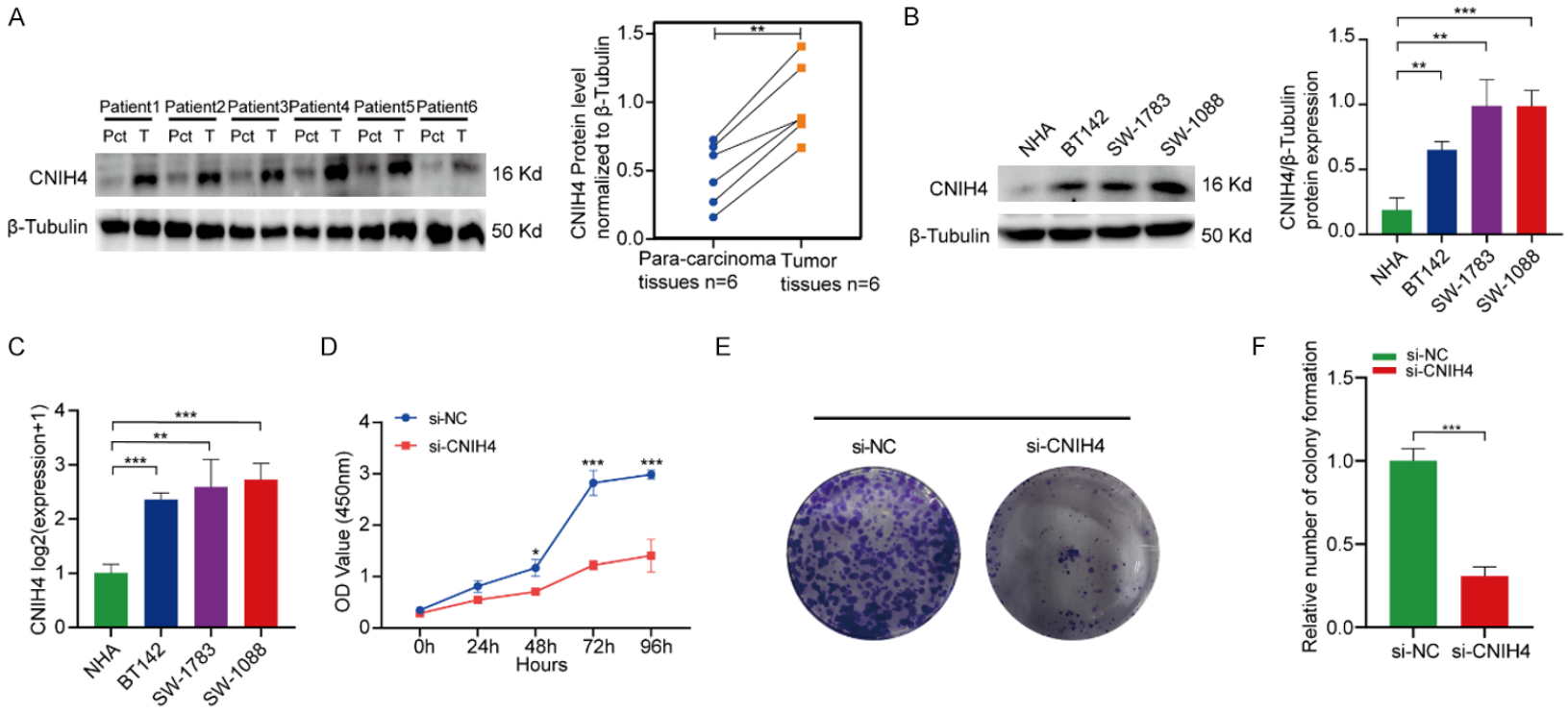
A
Patient1 Patient2 Patient3 Patient4 Patient5 Patient6
Pct T Pct T Pct T Pct T Pct T Pct T
CNIH4
β-Tubulin
16 Kd
50 Kd
CNIH4 Protein level normalized to β-Tubulin
Para-carcinoma tissues n=6
Tumor tissues n=6
B
NHA BT142 SW-1783 SW-1088
CNIH4
β-Tubulin
16 Kd
50 Kd
CNIH4/β-Tubulin protein expression
C
CNIH4 log2(expression+1)
D
si-NC
si-CNIH4
OD Value (450nm)
0h 24h 48h 72h 96h
Hours
E
si-NC
si-CNIH4
F
si-NC
si-CNIH4
Relative number of colony formation

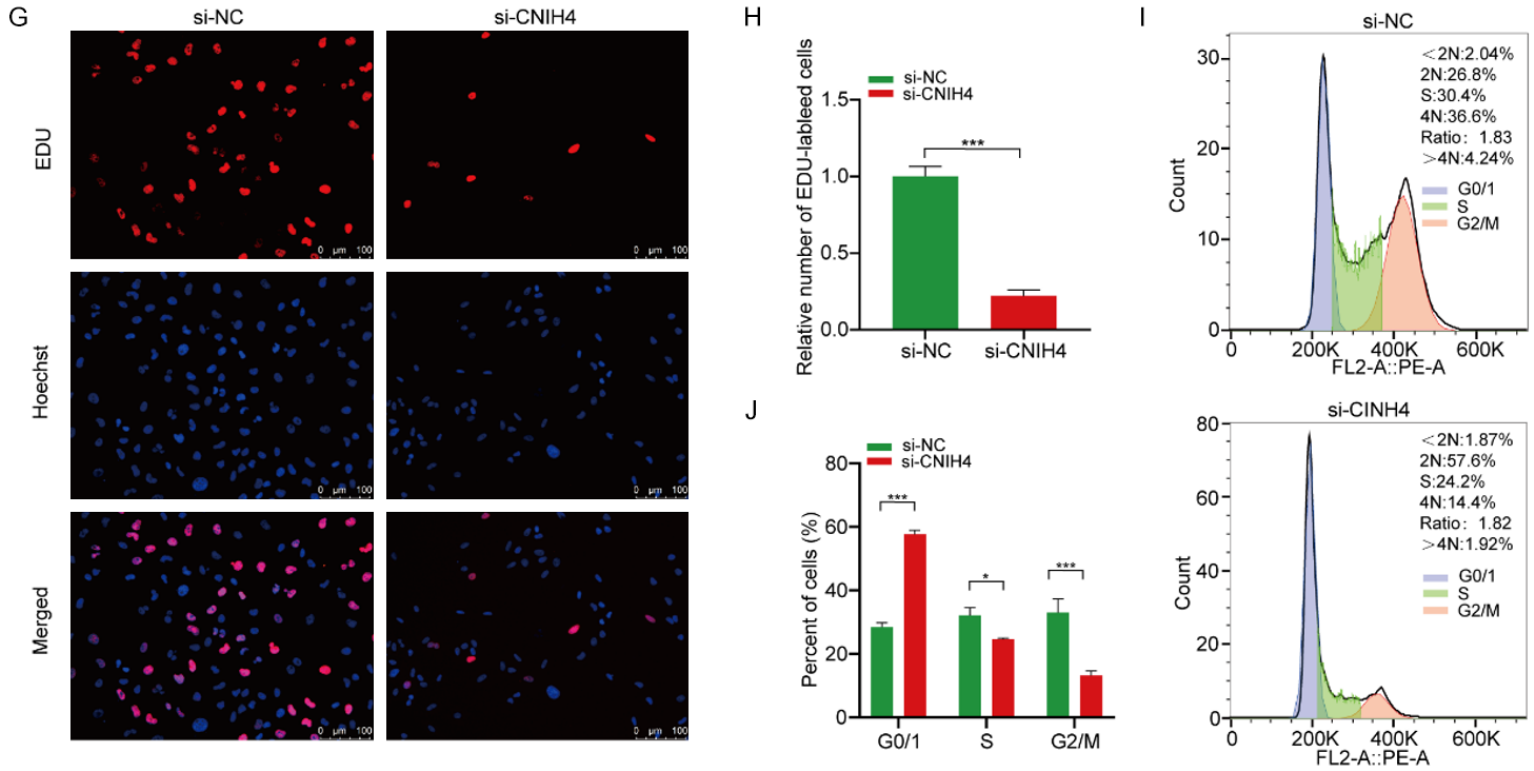

Figure 7. *In vitro* experimental verification of disruption of CNIH4 expression in LGG. A. Western blot analysis of CNIH4 expression in LGG and corresponding para-carcinoma tissues. B, C. Western blot and qRT-PCR analysis of CNIH4 expression in NHA and LGG cell lines. D. The cell viability of si-CNIH4-transfected and si-NC-transfected SW1088 cells by CCK-8 assays. E, F. Effect of CNIH4 knockdown on colony formation was counted in SW1088 cells. G, H. EdU assays were employed to inspect the cell proliferation after CNIH4 knockdown in SW1088 cells. I, J. Cell cycle assays were executed to detect the cell distribution of the SW1088 cell lines after CNIH4 knockdown. $^{*}P < 0.05$, $^{**}P < 0.01$, $^{***}P < 0.001$.

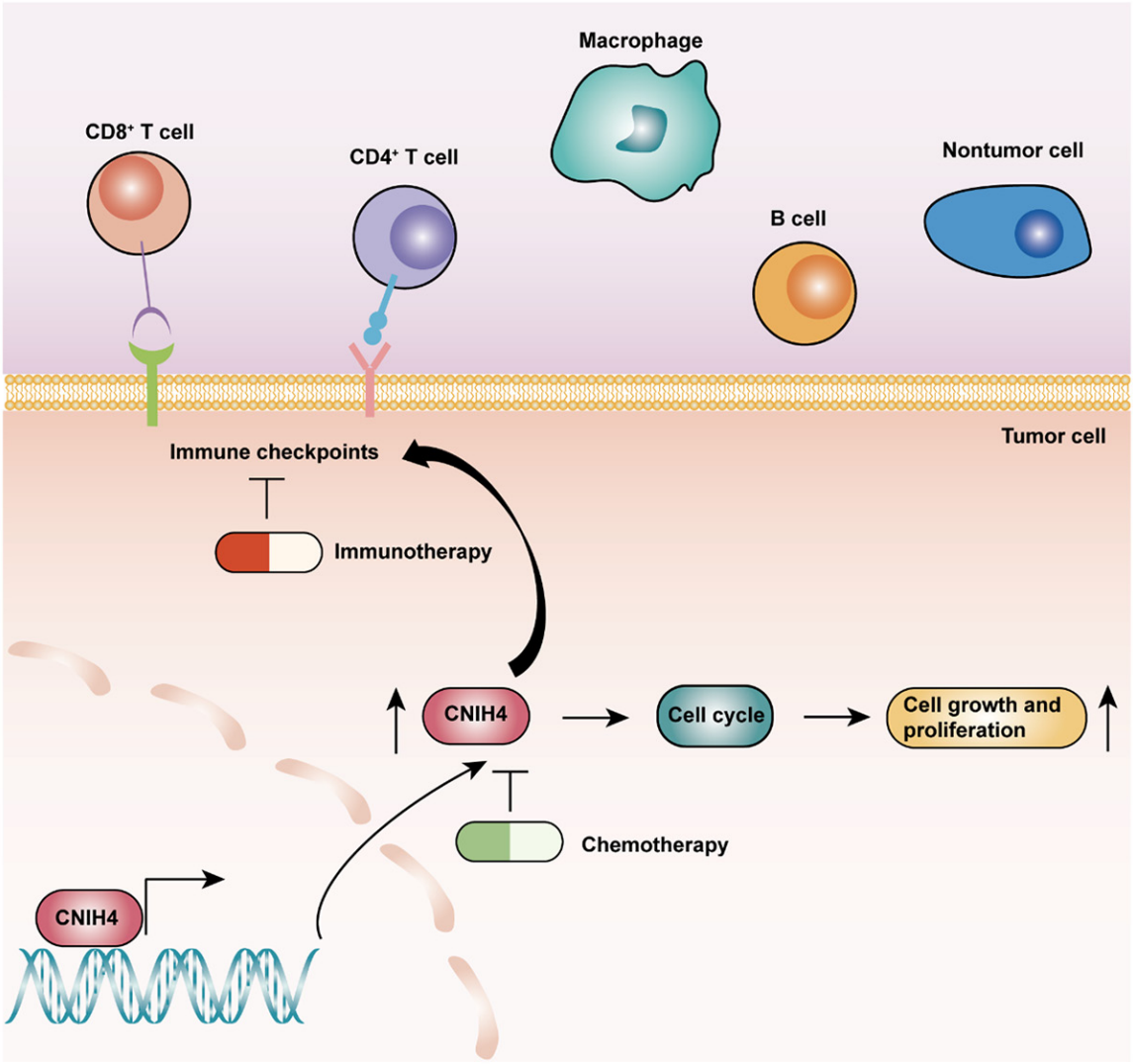

Figure 8. The biological mechanism underlying CNIH4 activity in LGG.

ever, the precise value of CNIH4 in patients with LGG remains to be elucidated. In this research, we comprehensively inspected the relationships among CNIH4 expression, clinical features, prognosis, biological function, immune traits, gene variations, and treatment response in patients with LGG.

First, we implemented pan-cancer analysis of CNIH4 in 33 cancers. The results illustrated that higher CNIH4 expression was associated with worse OS of pan-LGG patients, as well as higher expression of ICPGs and higher TMB. To determine whether CNIH4 has prognostic value in LGG, we carried out survival analysis using TCGA cohort data and found that patients in the high-CNIH4 expression subtype had worse prognosis than those in the low-CNIH4 expression subgroup. We also examined the OS rate of patients with LGG, and the results indicated that upregulation of CNIH4 expression was related to inferior OS status. ROC curves and AUC values were exploited to assess the value of CNIH4 for predicting the prognosis of patients with LGG. Evaluation of associations between CNIH4 expression and relevant clinical characteristics further suggested that there were clear differences in some clinical factors, including age, WHO grade, 1p/19q codel status, IDH, and MGMT. Additionally, Cox regression analyses illustrated that CNIH4 was an independent prognostic biomarker for LGG.

These results were all further validated in the CGGA dataset. Therefore, CNIH4 potentially represents a powerful prognostic biomarker in patients with LGG.

GO-BP and KEGG analysis of up-regulated DEGs in TCGA cohort indicated that they were enriched in PI3K-Akt signaling, the cell cycle, MAPK signaling, TNF signaling, leukocyte transendothelial migration, NF-kappa B signaling, and B cell receptor signaling. In addition, GSVA illustrated that high-CNIH4 expression was strongly connected with immune responses and cancer-associated signaling pathways. These results were also validated in the CGGA cohort. Hence, CNIH4 may promote the malignant progression of LGG by activating cancer-related signaling pathways.

The glioma immune microenvironment includes tumor cells, immune cells, and diverse cytokines [24], and there is a growing body of research supporting an essential role for the glioma immune microenvironment in glioma progression, metastasis, and drug resistance [25, 26]. Therefore, we exploited the ssGSEA algorithm to compare immune-related signatures between the low- and high-CNIH4 subtypes in TCGA and CGGA cohort data. The ESTIMATE and CIBERSORT algorithms were also implemented to compare tumor microenvironment (TME) composition and TIICs between the two subtypes. CNIH4 expression was tightly linked to immune infiltration in patients with LGG in both TCGA and CGGA cohorts. Immunotherapy has emerged as a new tumor treatment method, supported by extensive research, which acts by activating specific immune cells in the TME [27-29]. In particular, immune checkpoint inhibitors are new immunotherapy drugs used to treat different types of tumors with good efficacy [30-33]. Therefore, we evaluated the relationships between expression of CNIH4 and that of ICPGs in patients with LGG and found that CNIH4 expression was positively correlated with that of some notable ICPGs, including CD28, CD80, CD86, CTLA4, PD1, and PD-L1, in both TCGA and CGGA cohort data.

Genomic alterations may predict the prognosis and clinical immunotherapy response of patients with LGG [34, 35]. Thus, it is important to evaluate the relationship between CNIH4 expression and genomic alterations in patients with LGG. In this research, somatic mutation and CNA analyses demonstrated that patients in the high-CNIH4 subgroup tended to bear higher TMB and CNA burdens than those in the low-CNIH4 subgroup. Overall, our data indicate that CNIH4 may play a significant role in immunotherapy for patients with LGG. The molecular mechanisms potentially underlying the roles of CNIH4 in LGG are presented in **Figure 8**.

At present, temozolomide is the most common drug used for treatment of patients with LGG; however, its efficacy is restricted. Therefore, it is urgent to find new chemotherapy drugs to treat patients with LGG. Analysis of sensitivity to chemotherapy drugs revealed that the high-CNIH4 expression subtype was predicted to be more sensitive to chemotherapy drugs, including A-443654, CAL-101, AKT inhibitor VIII, TGX-221, MG-132, bortezomib, Bryostain-1, and TAK-175, than the low-CNIH4 expression subtype. Additionally, we performed drug sensitivity assays to validate the predicted difference in sensitivity to chemotherapy drugs between LGG with differential CNIH4 expression. Thus, CNIH4 may be a potential predictor of chemosensitivity in patients with LGG.

In addition to the bioinformatics analyses described above, we conducted *in vitro* experiments to confirm that CNIH4 was upregulated and played an essential role in cell proliferation, migration, invasion, and the cell cycle in LGG. However, this study has some limitations. First, the underlying molecular mechanisms involving CNIH4 in LGG should be investigated by conducting *in vivo* and additional *in vitro* experiments in the future. Second, further studies should be executed to examine whether CNIH4 can be an effective therapeutic target in patients with LGG.

Conclusion

Overall, our study indicates that CNIH4 is a reliable prognostic biomarker that is strongly associated with cell proliferation and the cell cycle in LGG. Moreover, CNIH4 may be an important therapeutic target in patients with LGG.

Acknowledgements

We sincerely appreciate all authors for their contributions. This research was supported by

Health Commission of Jiangxi Province (No. 202130356), and Education Department of Jiangxi Province (No. GJJ200178), Graduate Innovative Special Fund Projects of Jiangxi Province (No. YC2022-B073).

Disclosure of conflict of interest

None.

Abbreviations

CNIH4, the human cornichon homologue 4; LGG, lower-grade glioma; ICPGs, immune checkpoint genes; CAN, copy number alteration; TMB, tumor mutation burden; WHO, World Health Organization; TCGA, the Cancer Genome Atlas; GPCR, G protein-coupled receptor; CGGA, Chinese Glioma Genome Atlas; *IDH*, isocitrate dehydrogenase; ssGSEA, single-sample GSEA; GTEx, Genotype-Tissue Expression; FPKM, Fragments Per Kilobase Million; TPM, transcripts per kilobase million; OS, overall survival; ROC, receiver operating characteristics; AUC, area under the curve; FDR, false-discovery rate; DEGs, differentially expressed genes; GO-BP, Gene Ontology biological process; KEGG, Kyoto Encyclopedia of Genes and Genomes; ATCC, American Type Culture Collection; PVDF, transferred it to polyvinylidene fluoride; ECL, enhanced chemiluminescence; qRT-PCR, quantitative Real-Time PCR; IC50, lower inhibitory centration.

Address correspondence to: Drs. Hua Guo and Kai Huang, Department of Neurosurgery, The Second Affiliated Hospital of Nanchang University, Nanchang 330006, Jiangxi, China. Tel: +86-18979166606; E-mail: ndefy02014@ncu.edu.cn (HG); Tel: +86-19979928326; E-mail: kaihuang@ncu.edu.cn (KH)

References

[1] Yang K, Wu Z, Zhang H, Zhang N, Wu W, Wang Z, Dai Z, Zhang X, Zhang L, Peng Y, Ye W, Zeng W, Liu Z and Cheng Q. Glioma targeted therapy: insight into future of molecular approaches. Mol Cancer 2022; 21: 39.

[2] Louis DN, Perry A, Wesseling P, Brat DJ, Cree IA, Figarella-Branger D, Hawkins C, Ng HK, Pfister SM, Reifenberger G, Soffietti R, von Deimling A and Ellison DW. The 2021 WHO classification of tumors of the central nervous system: a summary. Neuro Oncol 2021; 23: 1231-1251.

[3] Mishra S, Bernal C, Silvano M, Anand S and Ruiz I Altaba A. The protein secretion modulator TMED9 drives CNIH4/TGFalpha/GLI signaling opposing TMED3-WNT-TCF to promote colon cancer metastases. Oncogene 2019; 38: 5817-5837.

[4] Wang Z, Pan L, Guo D, Luo X, Tang J, Yang W, Zhang Y, Luo A, Gu Y and Pan Y. A novel five-gene signature predicts overall survival of patients with hepatocellular carcinoma. Cancer Med 2021; 10: 3808-3821.

[5] Ritchie ME, Phipson B, Wu D, Hu Y, Law CW, Shi W and Smyth GK. Limma powers differential expression analyses for RNA-sequencing and microarray studies. Nucleic Acids Res 2015; 43: e47.

[6] Yu G, Wang LG, Han Y and He QY. clusterProfiler: an R package for comparing biological themes among gene clusters. OMICS 2012; 16: 284-287.

[7] Hanzelmann S, Castelo R and Guinney J. GSVA: gene set variation analysis for microarray and RNA-seq data. BMC Bioinformatics 2013; 14: 7.

[8] Barbie DA, Tamayo P, Boehm JS, Kim SY, Moody SE, Dunn IF, Schinzel AC, Sandy P, Meylan E, Scholl C, Frohling S, Chan EM, Sos ML, Michel K, Mermel C, Silver SJ, Weir BA, Reiling JH, Sheng Q, Gupta PB, Wadlow RC, Le H, Hoersch S, Wittner BS, Ramaswamy S, Livingston DM, Sabatini DM, Meyerson M, Thomas RK, Lander ES, Mesirov JP, Root DE, Gilliland DG, Jacks T and Hahn WC. Systematic RNA interference reveals that oncogenic KRAS-driven cancers require TBK1. Nature 2009; 462: 108-112.

[9] Yoshihara K, Shahmoradgoli M, Martinez E, Vegesna R, Kim H, Torres-Garcia W, Trevino V, Shen H, Laird PW, Levine DA, Carter SL, Getz G, Stemke-Hale K, Mills GB and Verhaak RG. Inferring tumour purity and stromal and immune cell admixture from expression data. Nat Commun 2013; 4: 2612.

[10] Newman AM, Liu CL, Green MR, Gentles AJ, Feng W, Xu Y, Hoang CD, Diehn M and Alizadeh AA. Robust enumeration of cell subsets from tissue expression profiles. Nat Methods 2015; 12: 453-457.

[11] Morad G, Helmink BA, Sharma P and Wargo JA. Hallmarks of response, resistance, and toxicity to immune checkpoint blockade. Cell 2021; 184: 5309-5337.

[12] Auslander N, Zhang G, Lee JS, Frederick DT, Miao B, Moll T, Tian T, Wei Z, Madan S, Sullivan RJ, Boland G, Flaherty K, Herlyn M and Ruppin E. Publisher correction: robust prediction of response to immune checkpoint blockade therapy in metastatic melanoma. Nat Med 2018; 24: 1942.

[13] Zhang H, Meltzer P and Davis S. RCircos: an R package for Circos 2D track plots. BMC Bioinformatics 2013; 14: 244.

[14] Mayakonda A, Lin DC, Assenov Y, Plass C and Koeffler HP. Maftools: efficient and comprehensive analysis of somatic variants in cancer. Genome Res 2018; 28: 1747-1756.
[15] Skidmore ZL, Wagner AH, Lesurf R, Campbell KM, Kunisaki J, Griffith OL and Griffith M. GenVisR: genomic visualizations in R. Bioinformatics 2016; 32: 3012-3014.
[16] Geeleher P, Cox N and Huang RS. pRRophetic: an R package for prediction of clinical chemotherapeutic response from tumor gene expression levels. PLoS One 2014; 9: e107468.
[17] Andrews MC, Reuben A, Gopalakrishnan V and Wargo JA. Concepts collide: genomic, immune, and microbial influences on the tumor microenvironment and response to cancer therapy. Front Immunol 2018; 9: 946.
[18] Keenan TE, Burke KP and Van Allen EM. Genomic correlates of response to immune checkpoint blockade. Nat Med 2019; 25: 389-402.
[19] Jung H, Kim HS, Kim JY, Sun JM, Ahn JS, Ahn MJ, Park K, Esteller M, Lee SH and Choi JK. DNA methylation loss promotes immune evasion of tumours with high mutation and copy number load. Nat Commun 2019; 10: 4278.
[20] Sim HW, Galanis E and Khasraw M. PARP inhibitors in glioma: a review of therapeutic opportunities. Cancers (Basel) 2022; 14: 1003.
[21] Kannan S, Murugan AK, Balasubramanian S, Munirajan AK and Alzahrani AS. Gliomas: genetic alterations, mechanisms of metastasis, recurrence, drug resistance, and recent trends in molecular therapeutic options. Biochem Pharmacol 2022; 201: 115090.
[22] Choi S, Yu Y, Grimmer MR, Wahl M, Chang SM and Costello JF. Temozolomide-associated hypermutation in gliomas. Neuro Oncol 2018; 20: 1300-1309.
[23] Lombardi G, Barresi V, Castellano A, Tabouret E, Pasqualetti F, Salvalaggio A, Cerretti G, Caccese M, Padovan M, Zagonel V and Ius T. Clinical management of diffuse low-grade gliomas. Cancers (Basel) 2020; 12: 3008.
[24] Wang K, Wang J, Zhang J, Zhang A, Liu Y, Zhou J, Wang X and Zhang J. Ferroptosis in glioma immune microenvironment: opportunity and challenge. Front Oncol 2022; 12: 917634.
[25] Bao Z, Wang Y, Wang Q, Fang S, Shan X, Wang J and Jiang T. Intratumor heterogeneity, microenvironment, and mechanisms of drug resistance in glioma recurrence and evolution. Front Med 2021; 15: 551-561.
[26] Yan D, Li W, Liu Q and Yang K. Advances in immune microenvironment and immunotherapy of isocitrate dehydrogenase mutated glioma. Front Immunol 2022; 13: 914618.
[27] Vesely MD, Zhang T and Chen L. Resistance mechanisms to Anti-PD cancer immunotherapy. Annu Rev Immunol 2022; 40: 45-74.
[28] Peng S, Xiao F, Chen M and Gao H. Tumor-microenvironment-responsive nanomedicine for enhanced cancer immunotherapy. Adv Sci (Weinh) 2022; 9: e2103836.
[29] Kubli SP, Berger T, Araujo DV, Siu LL and Mak TW. Beyond immune checkpoint blockade: emerging immunological strategies. Nat Rev Drug Discov 2021; 20: 899-919.
[30] Sove RJ, Verma BK, Wang H, Ho WJ, Yarchoan M and Popel AS. Virtual clinical trials of anti-PD-1 and anti-CTLA-4 immunotherapy in advanced hepatocellular carcinoma using a quantitative systems pharmacology model. J Immunother Cancer 2022; 10: e005414.
[31] Yamaguchi H, Hsu JM, Yang WH and Hung MC. Mechanisms regulating PD-L1 expression in cancers and associated opportunities for novel small-molecule therapeutics. Nat Rev Clin Oncol 2022; 19: 287-305.
[32] Wu M, Huang Q, Xie Y, Wu X, Ma H, Zhang Y and Xia Y. Improvement of the anticancer efficacy of PD-1/PD-L1 blockade via combination therapy and PD-L1 regulation. J Hematol Oncol 2022; 15: 24.
[33] Lisi L, Lacal PM, Martire M, Navarra P and Graziani G. Clinical experience with CTLA-4 blockade for cancer immunotherapy: from the monospecific monoclonal antibody ipilimumab to probodies and bispecific molecules targeting the tumor microenvironment. Pharmacol Res 2022; 175: 105997.
[34] Cai J, Hu Y, Ye Z, Ye L, Gao L, Wang Y, Sun Q, Tong S, Yang J and Chen Q. Immunogenic cell death-related risk signature predicts prognosis and characterizes the tumour microenvironment in lower-grade glioma. Front Immunol 2022; 13: 1011757.
[35] Binder H, Willscher E, Loeffler-Wirth H, Hopp L, Jones DTW, Pfister SM, Kreuz M, Gramatzki D, Fortenbacher E, Hentschel B, Tatagiba M, Herrlinger U, Vatter H, Matschke J, Westphal M, Krex D, Schackert G, Tonn JC, Schlegel U, Steiger HJ, Wick W, Weber RG, Weller M and Loeffler M. DNA methylation, transcriptome and genetic copy number signatures of diffuse cerebral WHO grade II/III gliomas resolve cancer heterogeneity and development. Acta Neuropathol Commun 2019; 7: 59.

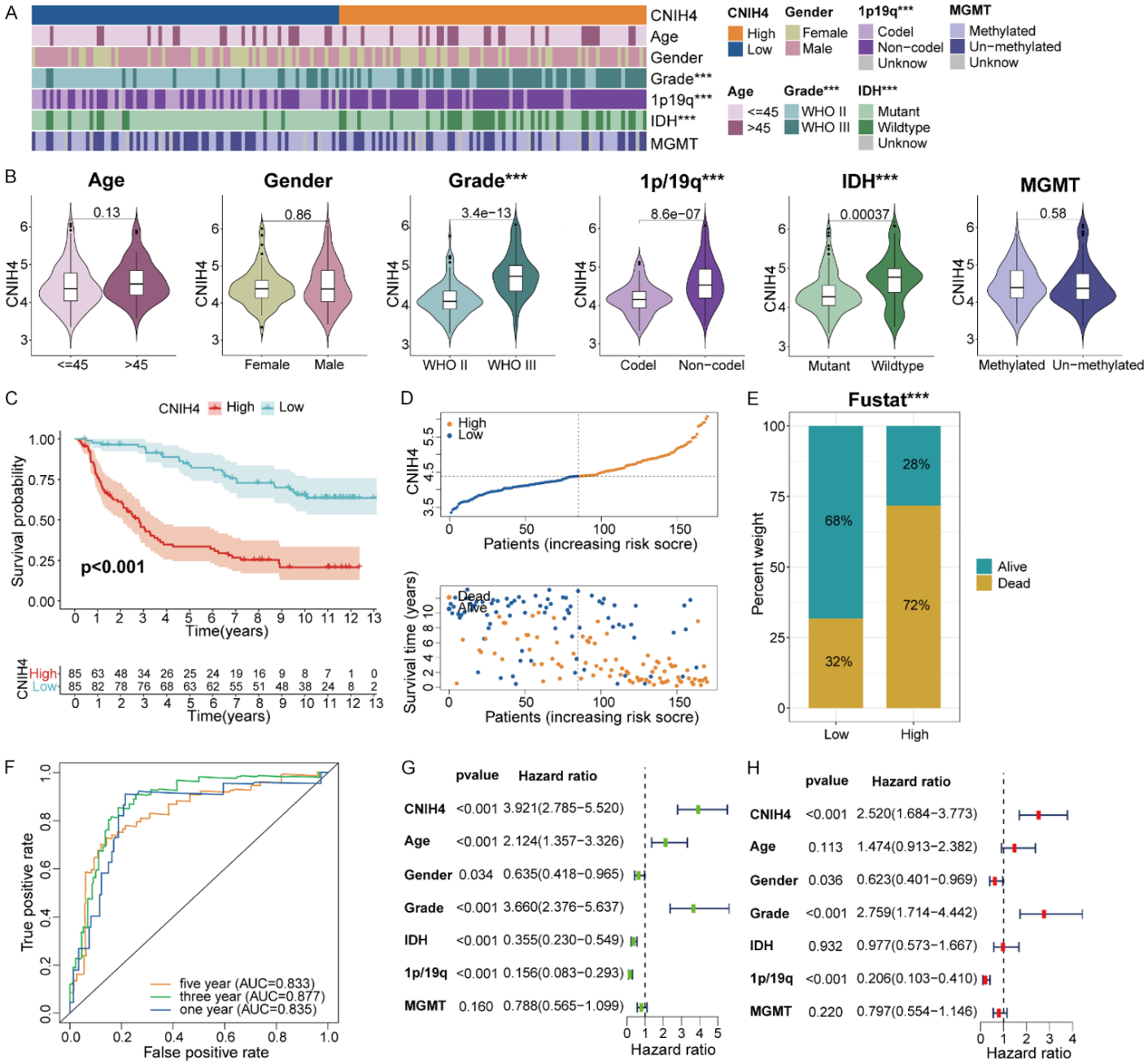
A
CNIH4
Age
Gender
Grade***
1p19q***
IDH***
MGMT
CNIH4 High Low
Gender Female Male
1p19q*** Codel Non−codel Unknow
MGMT Methylated Un−methylated Unknow
Age <=45 >45
Grade*** WHO II WHO III
IDH*** Mutant Wildtype Unknow
B
Age 0.13 <=45 >45
Gender 0.86 Female Male
Grade*** 3.4e−13 WHO II WHO III
1p/19q*** 8.6e−07 Codel Non−codel
IDH*** 0.00037 Mutant Wildtype
MGMT 0.58 Methylated Un−methylated
C
CNIH4 High Low
Survival probability
p<0.001
Time(years)
CNIH4 High 85 63 48 34 26 25 24 19 16 9 8 7 1 0
CNIH4 Low 85 82 78 76 68 63 62 55 51 48 38 24 8 2
Time(years)
D
High Low
CNIH4
Patients (increasing risk socre)
Dead Alive
Survival time (years)
Patients (increasing risk socre)
E
Fustat***
Percent weight
68%
32%
28%
72%
Low High
Alive Dead
F
True positive rate
False positive rate
five year (AUC=0.833)
three year (AUC=0.877)
one year (AUC=0.835)
G
pvalue Hazard ratio
CNIH4 <0.001 3.921(2.785−5.520)
Age <0.001 2.124(1.357−3.326)
Gender 0.034 0.635(0.418−0.965)
Grade <0.001 3.660(2.376−5.637)
IDH <0.001 0.355(0.230−0.549)
1p/19q <0.001 0.156(0.083−0.293)
MGMT 0.160 0.788(0.565−1.099)
Hazard ratio
H
pvalue Hazard ratio
CNIH4 <0.001 2.520(1.684−3.773)
Age 0.113 1.474(0.913−2.382)
Gender 0.036 0.623(0.401−0.969)
Grade <0.001 2.759(1.714−4.442)
IDH 0.932 0.977(0.573−1.667)
1p/19q <0.001 0.206(0.103−0.410)
MGMT 0.220 0.797(0.554−1.146)
Hazard ratio

Figure S1. Clinical correlation analysis of CNIH4 in CGGA. A. Associations between CNIH4 expression and clinical traits of patients with LGG in CGGA. B. Analysis of variance in CNIH4 expression in patients with different clinical features, including age, sex, tumor grade, and 1p/19q, *IDH*, and MGMT statuses, in the CGGA dataset. C. Prognostic analysis of high- and low-CNIH4 subtypes in the CGGA dataset. D. Distribution of risk score, OS, and OS status of high- and low-CNIH4 subtypes in the CGGA dataset. E. Comparison of survival rate between the two subtypes. F. ROC curves illustrating the predictive value of the risk score in CGGA data. G, H. Univariate and multivariate Cox analyses of CNIH4 expression and clinicopathological characteristics in CGGA data. $^{*}P < 0.05$, $^{**}P < 0.01$, $^{***}P < 0.001$.

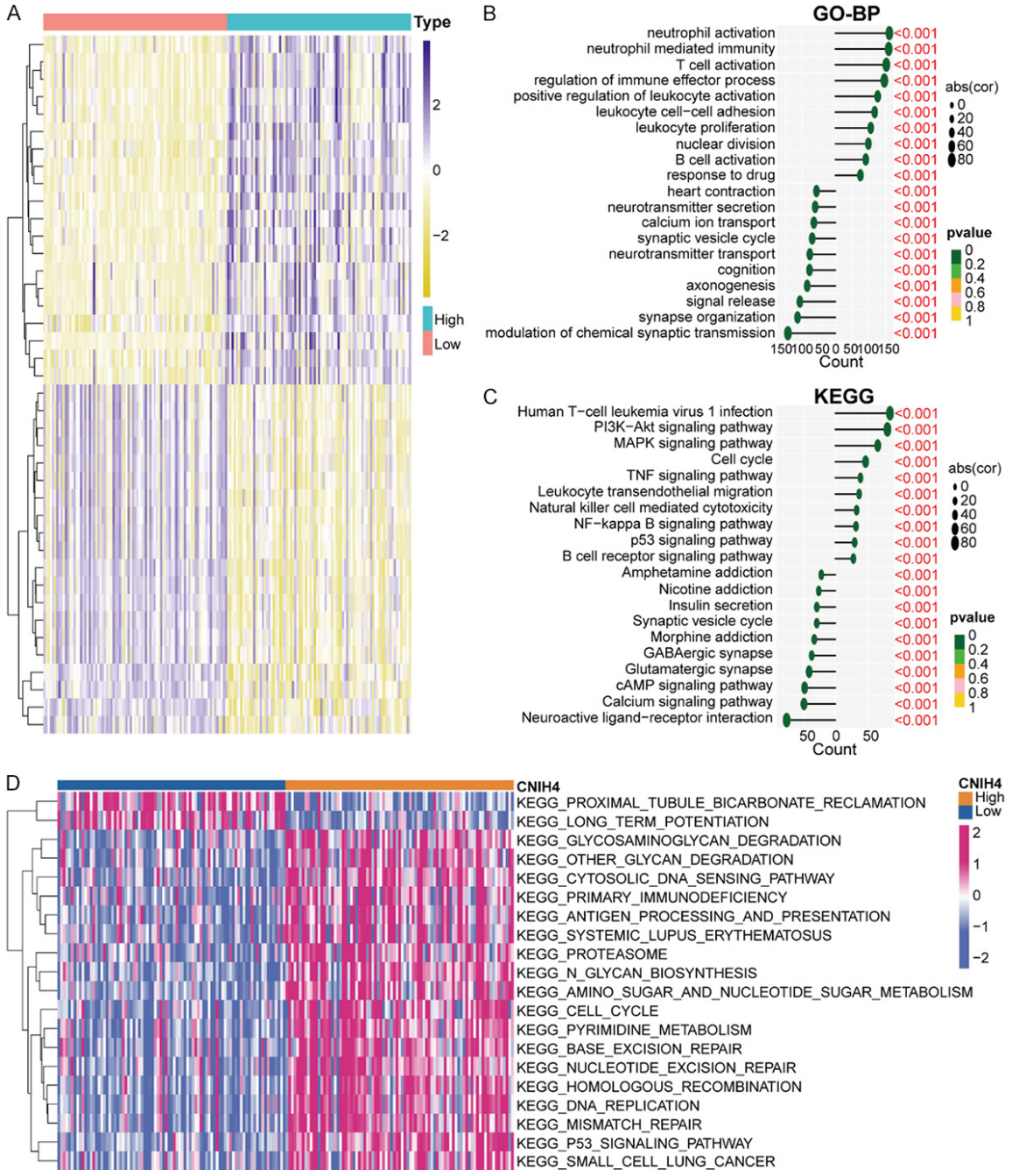

Figure S2. Biological functions of CNIH4 in LGG in CGGA. A. DEGs between the low- and high-CNIH4 expression LGG subgroups. B, C. GO-BP and KEGG analyses for CNIH4 expression-associated DEGs in patients with LGG in the CGGA dataset. D. GSVA of the CGGA dataset.

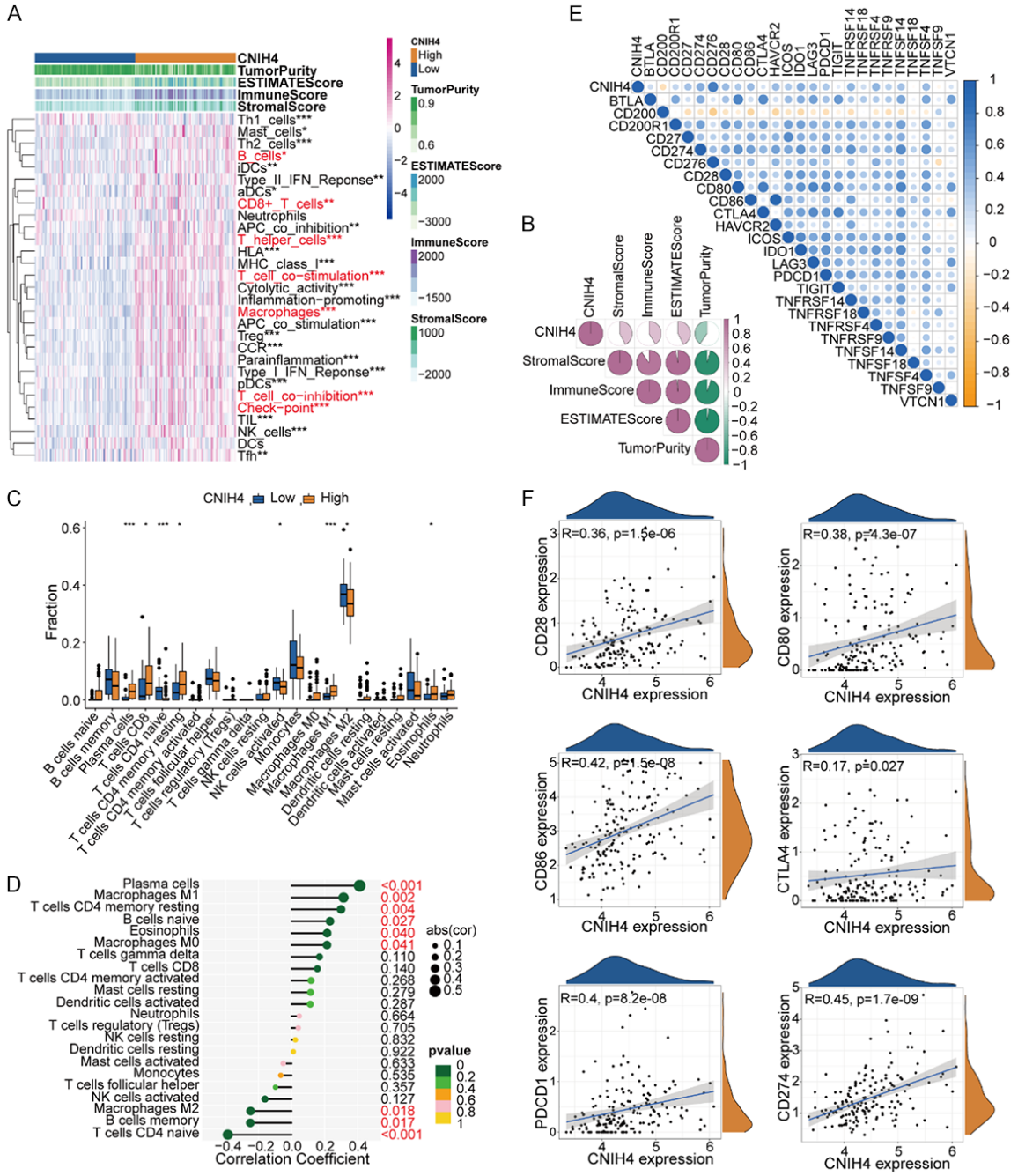

Figure S3. Different tumor microenvironment and immunological characteristics of the low- and high-CNIH4 subtypes in CGGA. A, B. Associations between CNIH4 expression and 29 immune-associated signatures, ESTIMATE, immune, stromal scores, and tumor purity. C. Comparisons of infiltration of 22 types of immune cell in the low- and high-CNIH4 LGG subgroups. D. Lollipop plots illustrating the relationship between CNIH4 expression and TIICs. E, F. Co-expression analysis of CNIH4 and 25 ICPGs. $^{*}P < 0.05$, $^{**}P < 0.01$, $^{***}P < 0.001$.

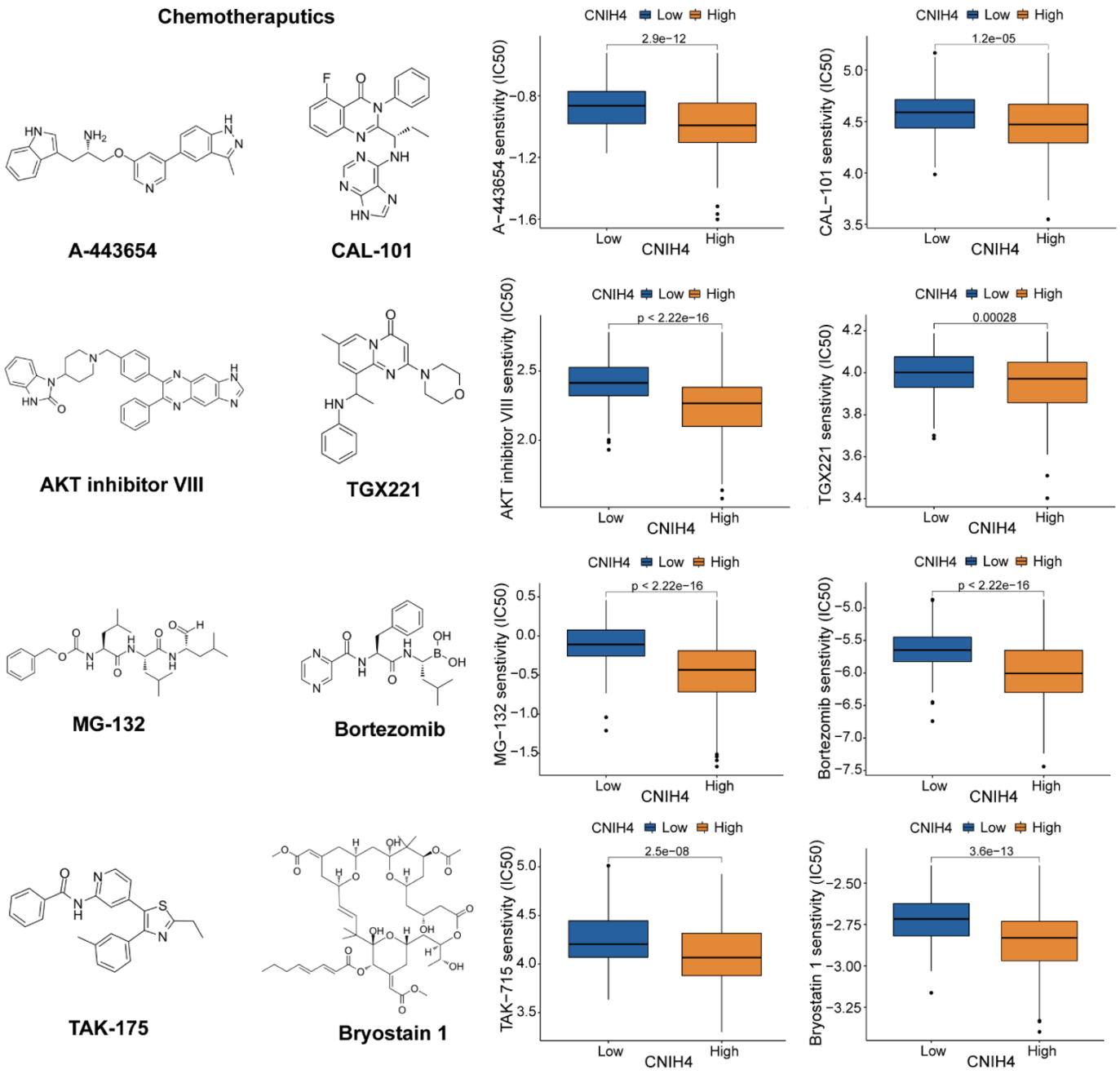
Chemotheraputics
A-443654
CAL-101
AKT inhibitor VIII
TGX221
MG-132
Bortezomib
TAK-715
Bryostain 1
CNIH4 Low High
2.9e−12
A−443654 senstivity (IC50)
1.2e−05
CAL−101 senstivity (IC50)
p < 2.22e−16
AKT inhibitor VIII senstivity (IC50)
0.00028
TGX221 senstivity (IC50)
MG−132 senstivity (IC50)
Bortezomib senstivity (IC50)
2.5e−08
TAK−715 senstivity (IC50)
3.6e−13
Bryostatin 1 senstivity (IC50)
Low
High
CNIH4

Figure S4. Comparisons of predicted responses to anticancer drugs, including A-443654, CAL-101, AKT inhibitor VIII, TGX-221, MG-132, bortezomib, Bryostain-1, and TAK-175, between the low- and high-CNIH4 subgroups in TCGA dataset.

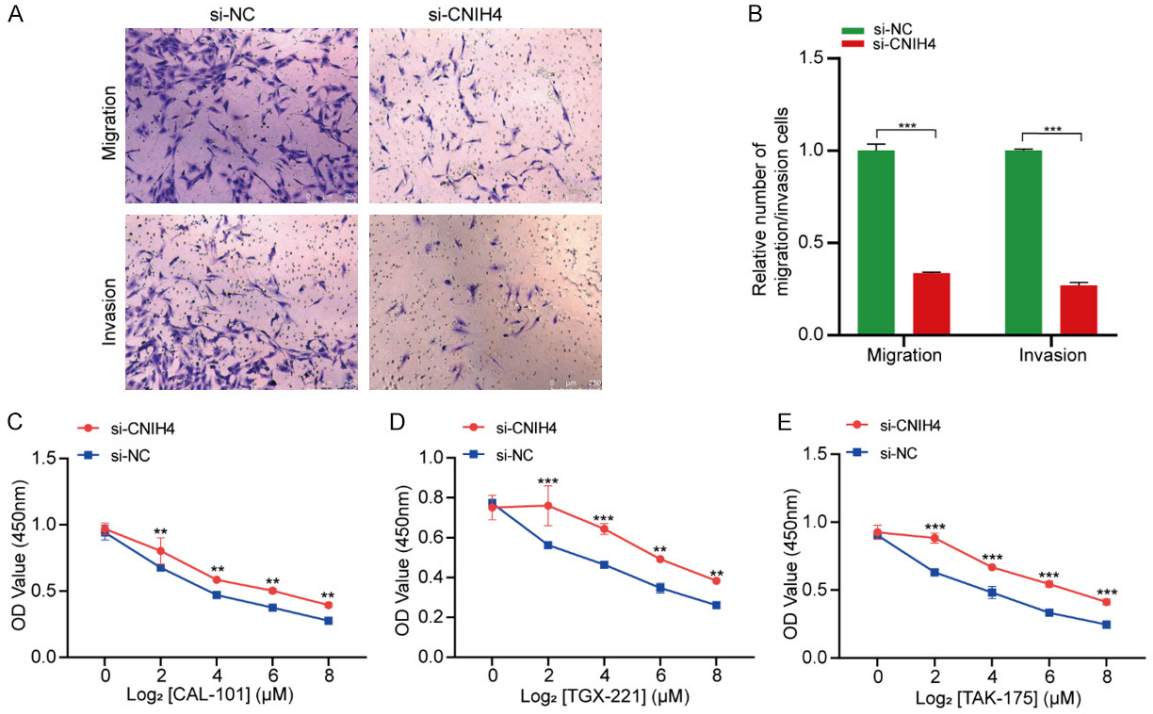

Figure S5. Confirmation of migration and invasion capacities of CNIH4 and drug sensitivity assays in LGG. A, B. Transwell assays after CNIH4 knockdown in SW1088 cells. C-E. Drug sensitivity assays between si-CNIH4-transfected and si-NC-transfected SW1088 cells. $^{*}P < 0.05$, $^{**}P < 0.01$, $^{***}P < 0.001$.